ANNUAL REPORT

on

THE RESEARCH AND DEVELOPMENT OF A SOLUBLE REACTANTS AND PRODUCTS SECONDARY BATTERY SYSTEM

NASA Grant NSG-3010**

May 1, 1974 - July 31, 1975

Submitted By

Chung-Chiun Liu*

Chemical and Petroleum Engineering Department
University of Pittsburgh
Pittsburgh, Pennsylvania 15261

*Principle Investigator and to whom to address all correspondence.

**The NASA Technical Officer for this Grant is Ms Patricia O'Donnell, Lewis Research Center, NASA, Cleveland, Ohio.

INTRODUCTION

The Chemical Engineering Department of the University of Pittsburgh is carrying out a 12-month research program to develop a soluble reactants and products secondary battery system.

The proposed secondary battery is based on a physical concept different from any presently used secondary battery system. The electrodes, electrolyte, reactants, and half-cell separators used in this system differ from those of conventional ones. Thus, any evaluation or analysis of the performance of the proposed system in terms of energy output, cost, etc. requires information which is presently not available. Furthermore, the essential battery-operating characteristics of this proposed redox system are not known. Thus, the following experimental studies are considered to be most critical in determining the success of this proposed secondary battery system.

1. Measurement of the essential physical and chemical properties of the reactants and products in the proposed redox systems;

2. Evaluation of commercially available anion membranes as the cell separator, determination of the composition and the degradation mechanism of the anion membrane, and/or developing an anion membrane separator; and

3. Evaluation of the battery performance of the prototype secondary battery systems based on this principle.

This research grant was formerly executed on May 1, 1974 by the Research Office of the University of Pittsburgh. Our work on this research lasted until July 31, 1975 including 3 months of no cost extension. This extension was granted by

NASA, because the principal investigator was involved in an accident and was unable to perform the work as planned.

In summary, we consider our research progressing well, and our results obtained in this research are invaluable in future development of secondary battery systems based on this redox principle.

EXPERIMENTAL RESULTS

Experimental Measurements of the Physical Properties of Selected Chloride Solutions Used in the Redox Coupled Secondary Battery Systems

The developing redox battery systems employ an aqueous electrolyte. These are metal chloride solutions. The physical properties of these chloride solutions may directly affect the performance of the battery systems as well as their optimum designs. Of all the physical properties of these chloride solutions, the following ones are of primary interest:

(1) solubility
(2) conductivity
(3) viscosity
(4) density
(5) surface tension
(6) boiling and freezing temperatures

These physical properties are directly related to the electrical characteristics and transport properties of the chloride solutions. Also, these physical properties are considered concentration dependent. Thus, the effects of the concentration on each of these properties will be examined experimentally. A description of our findings for each studied follows:

1. Solubility

The solubilities of employed metal chlorides in aqueous solution were measured in this study. Our methodology in making these measurements can be described as follows.

Hydrochloric acid, HCl, in 12N acidic strength was used to prepare different concentration levels of HCl solvents. The HCl was diluted with double distilled water. This diluted HCl solution was the solvent used in this study. For each run,

10 ml of the solvent was used. Volumetrically, the HCl (12N) to water ratio of the solvents prepared were 1:9, 3:7, 5:5, 7:3 and 9:1. These solvents represented a molar concentration of HCl of 1.2, 3.6, 6.0, 8.4, and 10.2, respectively. In some cases, 10 ml of distilled water and/or 10 ml of 12N HCl were used as solvents. The metal chlorides used were all reagent grade chemicals and were purchased from the Fisher Scientific Company, Pittsburgh, Pennsylvania.

In general, an amount of approximately 5 gms of the chloride was weighed. From this amount, a small portion of the chloride was gradually added into the solvent (solutions of different HCl strengths). Constant stirring and careful visual observation were essential in determining the degree of chloride dissolution. Once the chloride appeared to be insoluble in the solvent, the remaining portion of the chloride was calculated. The pH value of the solution was measured and compared to the value measured prior to any addition of the chloride. For most cases, the pH value of the solution changed slightly from those of the solvents. Nearly all of the prepared solutions exhibited strong acidic characteristics and had a pH value near or below zero.

The experimental data was then analyzed using a linear regression technique. A linear relation was obtained between the molar number of dissolved chloride and that of the HCl in the solvent. This linear relation was checked experimentally by making a second run. In this second run, the chloride solution was prepared according to the prediction of the linear relation. If, however, any discrepancy occurred between the results of the prediction and the preparation, the data used in construction the linear equation would be discarded. The experiment would be repeated.

All the solubility measurements were performed at room temperature, ~ 20°C. The measured solubilities were also compared to reported data whenever available. Information reported by Linke[1] was used extensively.

Figures 1 and 2 present the solubilityof the ferrous chloride ($FeCl_2$) and ferric chloride ($FeCl_3$) at ~ 20°C respectively. For $FeCl_2$, our experimental measurements agree substantially well with those reported by Linke. For $FeCl_3$, the data reported by Linke was relatively sporadic and only certain points agree with our experimental results.

Figures 3 and 4 present the solubility of the cuprous chloride (CuCl) and cupric chloride ($CuCl_2$) at ~ 20°C respectively. For the CuCl, the maximum dissolution is 2.7 molar in a solvent of 10.5 molar HCl solution. Our data agrees well with those reported by Linke. For chromium salts, the solubility measurements were experimentally difficult. In the case of chromic chloride, $CrCl_3 \cdot 6H_2O$, the coexisting hydrated forms of chromic chloride resulted in the difficulty of this study. At low temperature, hydrated chromic chlorides exist in the forms of $[CrCl_2(H_2O_4]Cl \cdot 2HO$ (dark green), $[CrCl(H_2O)_5]Cl_2 \cdot H_2O$ (light green) and $[Cr(H_2O)_6]Cl_3$ (violet).[2] At room temperature and over a concentration of 3 - 68.5 wt% of $CrCl_3 6H_2O$, the dark green and the violet hexahydrates are at equilibrium and have different equilibrium concentrations. When HCl is added to an aqueous solution, the dissolution of the green hexahydrate chromic chloride becomes more favorable. Yet the increase of HCl in the solvent will precipitate the violet form of chromic chloride to a greater extent. These opposite effects made the solubility measurement of chromic chloride in different HCl strength aqueous solution complicated and difficult to interpret the results.

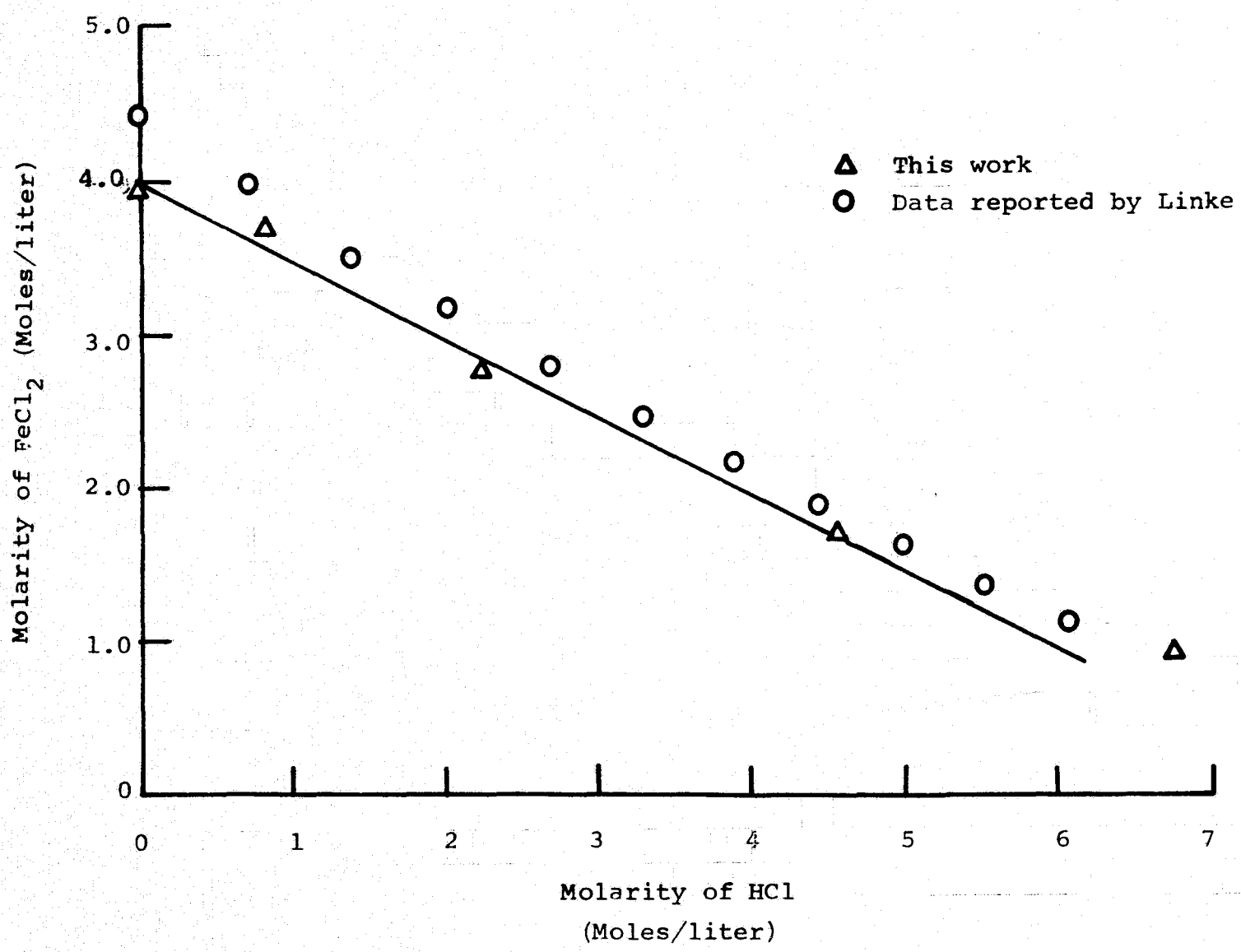

FIGURE 1 : Solubility of the Ferrous Chloride as a Function of Hydrochloric Acid at ~ 20°C

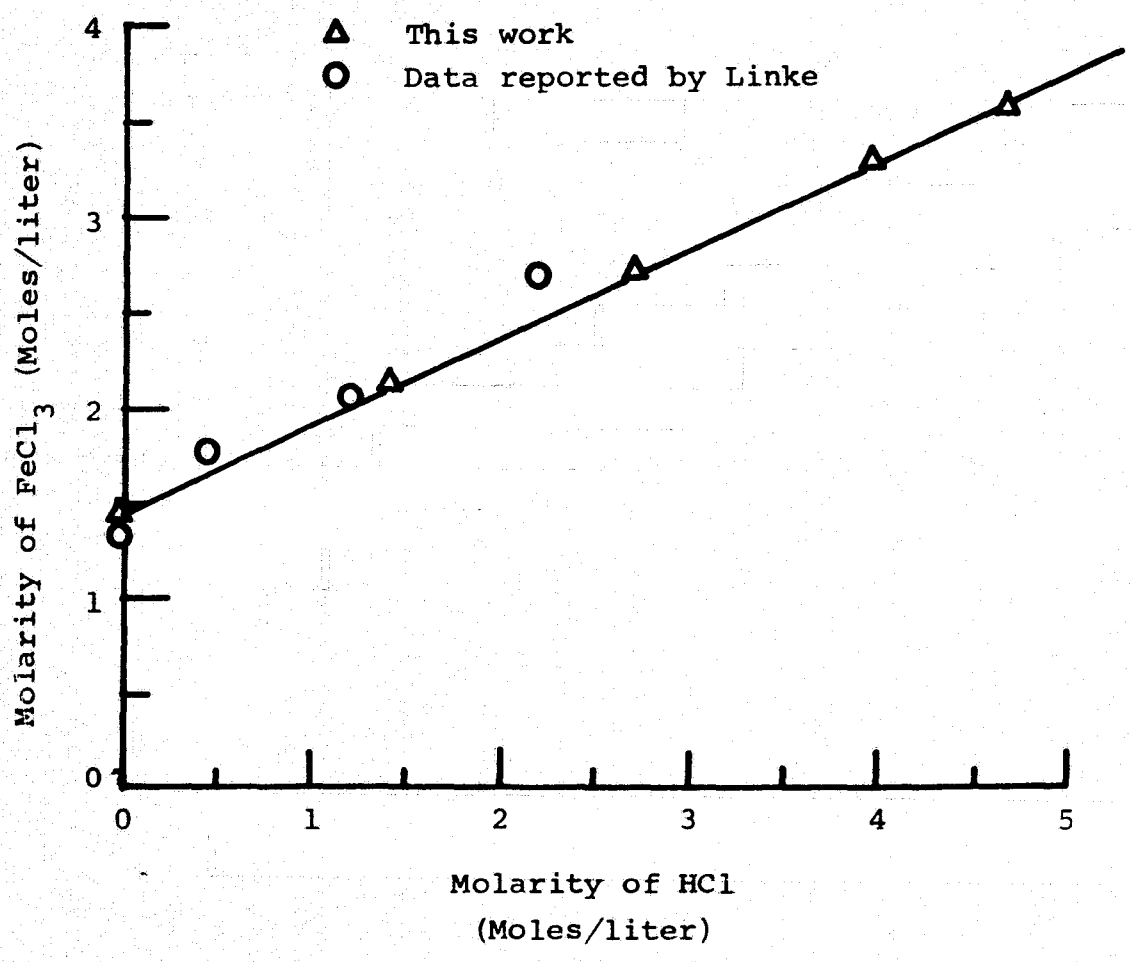

FIGURE 2 : Solubility of the Ferric Chloride as a Function of Hydrochloric Acid at ~ 20°C

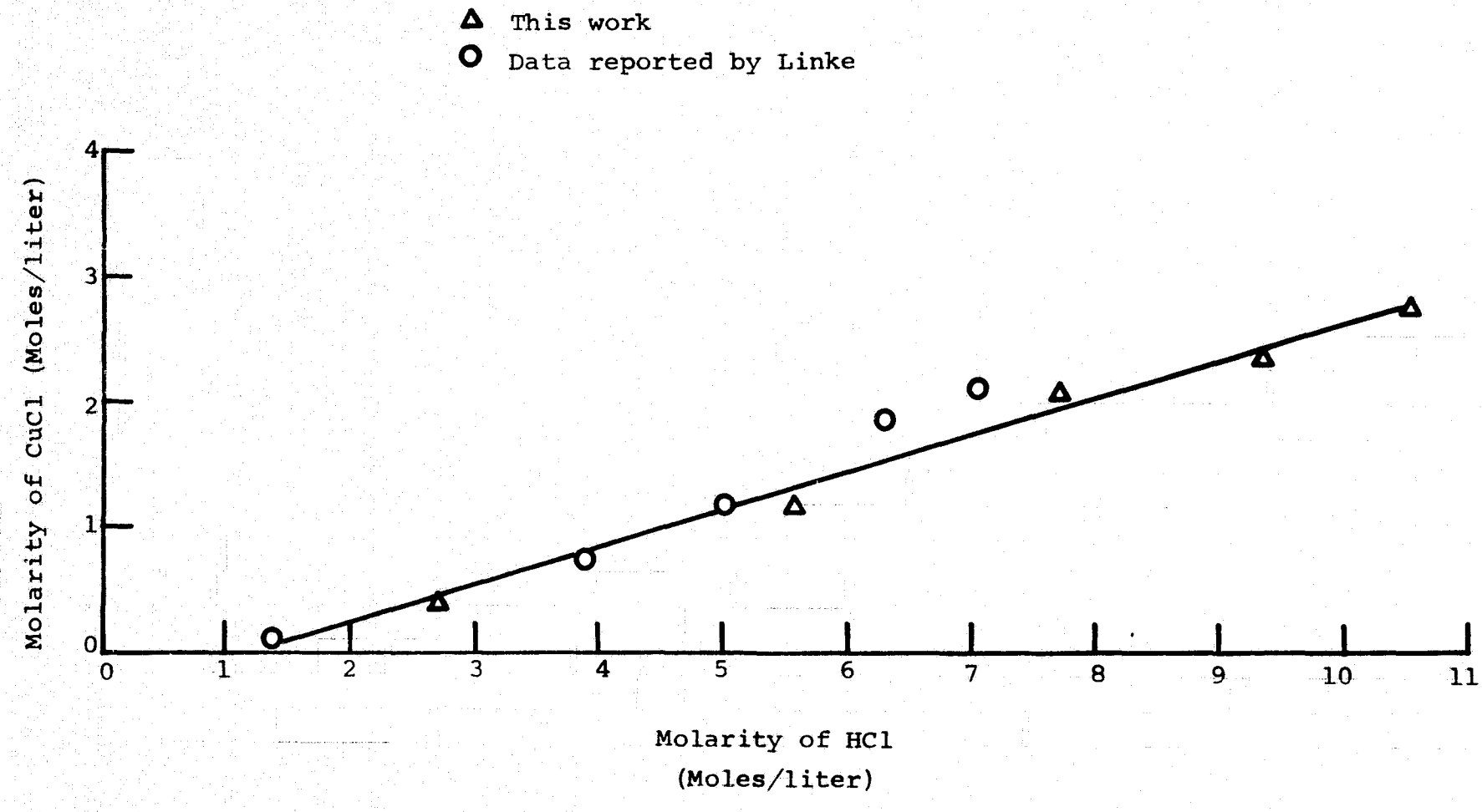

FIGURE 3 : Solubility of the Cuprous Chloride as a Function of Hydrochloric Acid at ~ 20°C

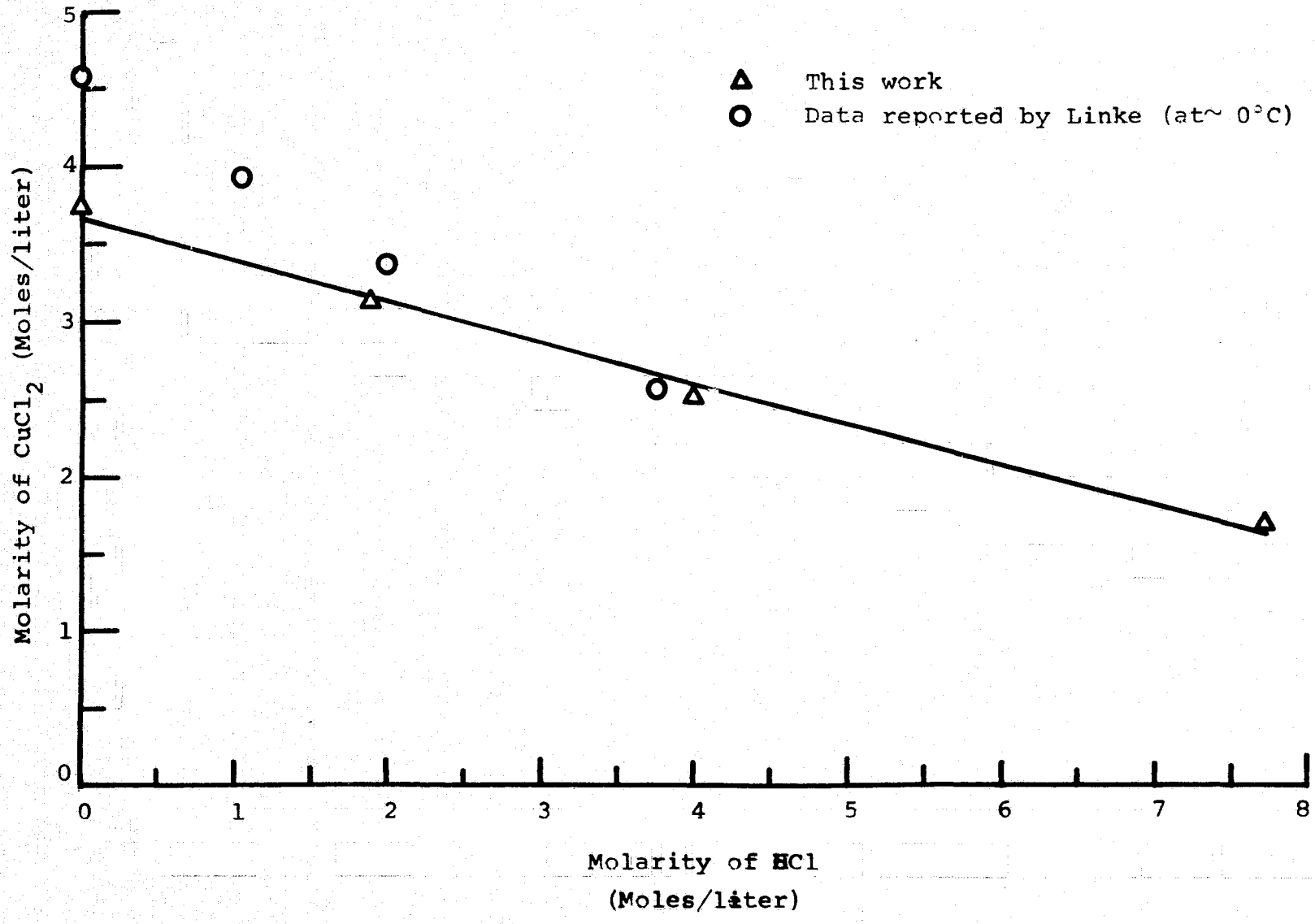

FIGURE 4 : Solubility of the Cupric Chloride as a Function of Hydrochloric Acid at ~ 20°C

In our study, the experiment was carried out in a nitrogen-filled dry box as well as in room air. Their results were compared. Chromic chloride received was in the form of chunks. Normally, the chromic chloride was finely ground first for easy handling. This grounding process might dehydrate the molecular water of the chromic chloride, and dehydrated chromic chloride was considered insoluble in aqueous solution. Thus, the chromic chloride was then used without grounding. The results of these precautions and modifications in the experimental procedure proved to be marginal. The solubility measurements of chromic chloride were uncertain due to its different hydrated forms and different responses to the HCl in the solution.

According to Linke[1] and other literature,[3] $CrCl_3 \cdot 6H_2O$ has a solubility of ~ 3.9 molar in water. Our experimental measurements agree with this reported value though our measurements are, quantitatively, slightly lower. One must also realize that the different hydrated forms of the chromic chloride also affect the electrical conductivity and density[4] of the chromic chloride solution. This makes the other physical properties of the chromic chloride equally complicated.

For chromous chloride, the unstability of the chromous solution toward air is the major cause of difficulty in the solubility measurements. In our study, a nitrogen filled dry box was employed. However, as expected, when HCl was added in the water as a solvent, the available hydrogen ions oxidized the solution. Consequently, this oxidation alters the chromous ions (to various hydrated forms of chromic chloride) and makes any further measurement undefinable.

Previously, Stone and Beeson[5] prepared volumetric solutions of chromous salts by reducing solutions of violet chrome alum in a Jones reductor. Lingane and Pecsok[6] prepared chromous solutions by reduction of appropriate quantities of pure potassium dichromate with zinc mossy amalgamated with 1% mercury. Hydrogen or carbon dioxide were generally used to maintain an inert atmosphere. Recently, a modified method proposed by Williams and Sill[7] appeared to be relatively simple. In this method, a mercury chloride solution was first prepared, then zinc shot was added into the solution and formed an amalgamated zinc. This amalgamated zinc was then used to reduce chromic chloride solution forming chromous chloride solution. All these methods, however, prepared the chromous chloride solution having a concentration of only 0.5M strength. Higher concentration-level chromous chloride solutions have never been prepared in this manner. The equilibrium constant between chromic ions and chromous ions at room temperature will govern the highest attainable concentration of the chromous chloride solution prepared in this manner. In this study, a chromous solution was purchased directly (So-C-169 Fisher Scientific Co.). This solution was titrated with alkali solution, NaOH, to precipitate the chromous ions (in the form of chromous hydroxide). The results show that, at least, a 3.61 molar chromous solution can be prepared.

For titanium ions, a 20 wt% titanous chloride solution was available commercially (Fisher Scientific Co., Pittsburgh, PA, Item SO-T-43). The titanous ions in the solution were also titrated with dosium hydroxide solution. The precipitated hydroxide was weighed, and the molarity of

the chloride solution calculated accordingly. A molar value of 1.87 for the titanous chloride solution was obtained. For titaniumic tetrachloride, $TiCl_4$ was directly made from titanium metal with HCl. In an oxygen-free environment, the titaniumic tetrachloride was purplish in color. However, the solution became yellowish once it contacted air, (oxygen) thereby affecting the solubility. At room temperature, the rate of direct dissolution of titanium in hydrochloric acid is very slow. Whereas at elevated temperatures, this rate of dissolution increases. We found that for concentrated HCl(12N) a $\sim$ 1 molar titaniumic tetrachloride solution could be prepared. This value may not be the maximum solubility of the titanium in HCl solution, since investigation is still being made. The color change in this study indicates that the titanium in HCl may have different forms. This requires further careful study regarding the actual solubility of the titanium in HCl.

Studies in stannous and stannic chloride yielded inconclusive results due to the instability of the chemicals in atmosphere.

Because of the indefined solubility of the titaniumic tetrachloride stannous and stannic chlorides, any of their other physical properties will not be reported until further clarification of the solubility of these compounds are completed.

2. Conductivity

The electrical conductivities of the chloride solutions are of importance in the developing redox battery systems. In this research, a Beckman conductivity bridge (Model RC16B2) was used for the conductivity measurement of each

chloride solution. The conductivity cell used had a cell constant, K value, of 2.00/cm. (Beckman 7056D-4). In each run, an amount of 40 ml of the solution was used. Both the resistance and the conductivity of the solution were measured experimentally using the conductivity bridge. Because the resistance is the reciprocal of the conductivity, its measurement provides a reference in confirming the conductivity measurement. The electrical conductivity is expressed as specific conductance, $(ohm\text{-}cm)^{-1}$.

The conductivities of the chloride solutions measured were all for saturated solutions. The conductivities were measured over the temperature range of 20-72°C. The specific conductivity was presented as a function of the molarity of the chloride solution. Figure 5-8 shows the specific conductivity of $FeCl_2$, $FeCl_3$, CuCl, and $CuCl_2$, respectively. As expected, for any specific chloride solution, the increase of temperature increases the specific conductivity. For the titanous chloride, the 20 wt% solution (1.87 molarity) with zero molar HCl was used in the conductivity measurement. Table 1 summarized the measurements.

TABLE 1

SPECIFIC CONDUCTANCE OF 20 WT% TITANOUS CHLORIDE

Temperature °C	22.3	29.9	48.9	71.7
Specific Conductance $(ohm\text{-}cm)^{-1}$	0.149	0.167	0.178	0.181

3. Viscosity

The kinematic viscosity of the chloride solution was measured using Cannon-Fenske viscometer. All the viscometers were calibrated and calibration constant certified. The viscosity measurements were done in a constant temperature bath

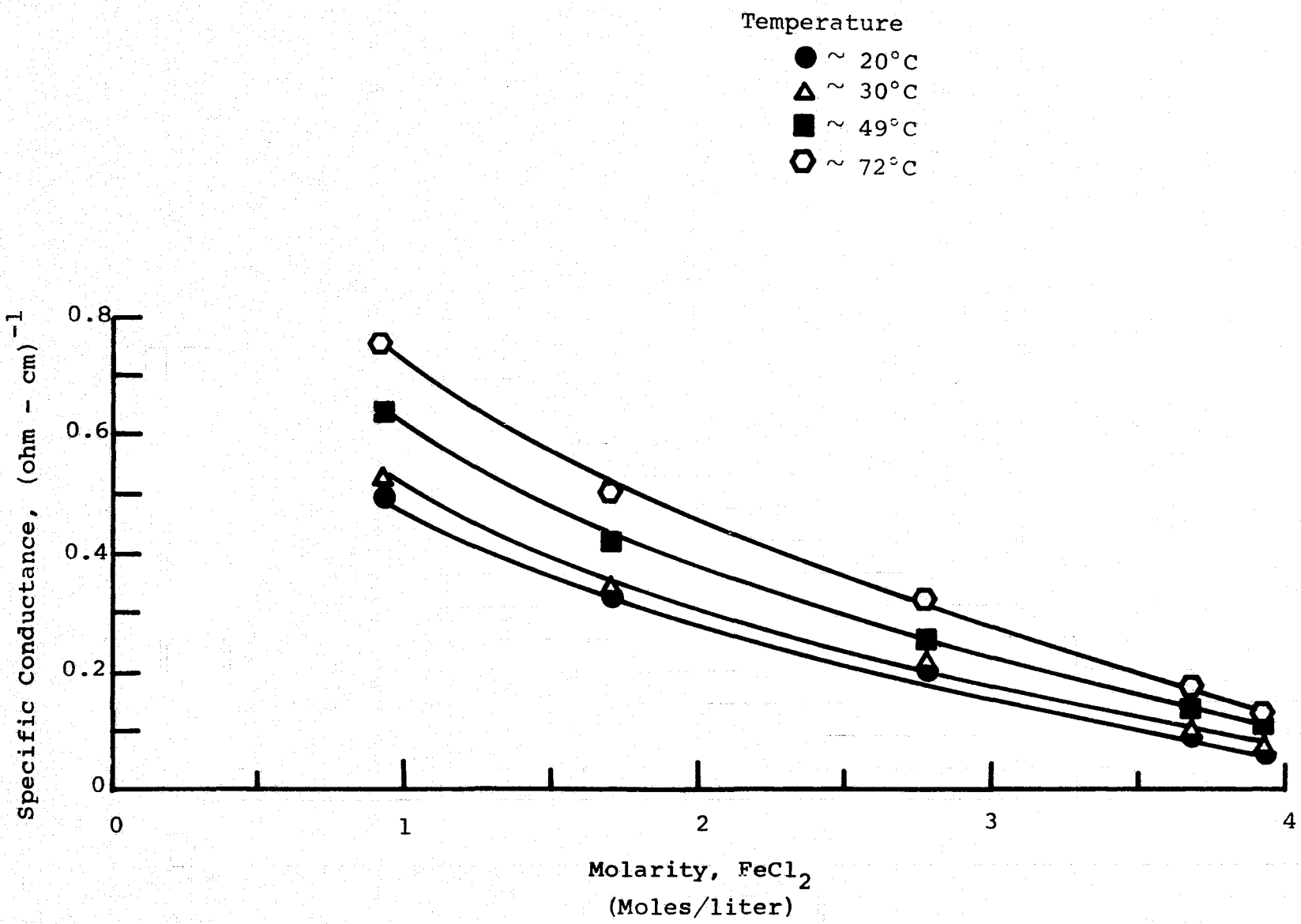

FIGURE 5 : Specific Conductances of the Ferrous Chloride Solutions at Different Temperatures

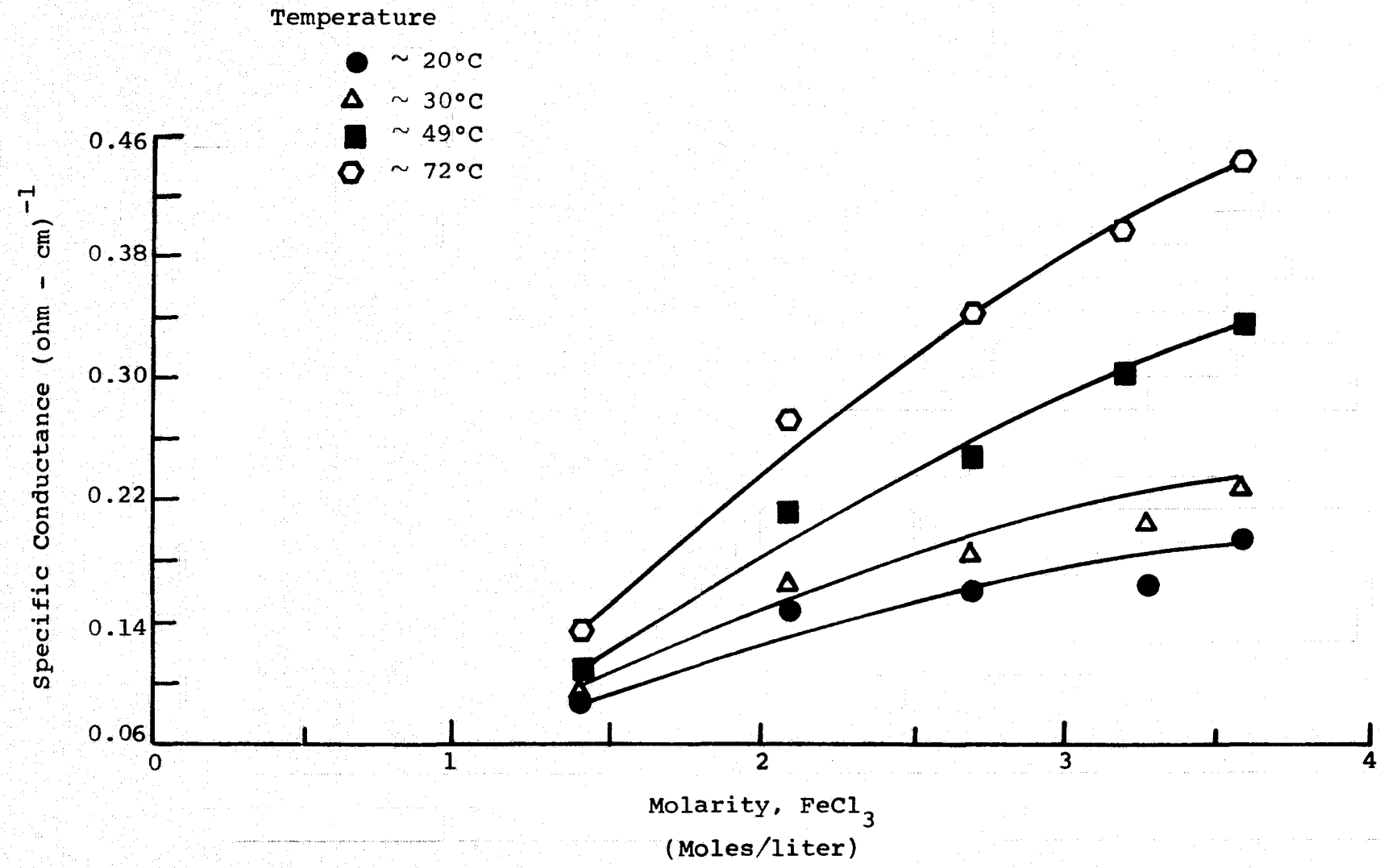

FIGURE 6: Specific Conductances of the Ferric Chloride Solutions at Different Temperatures

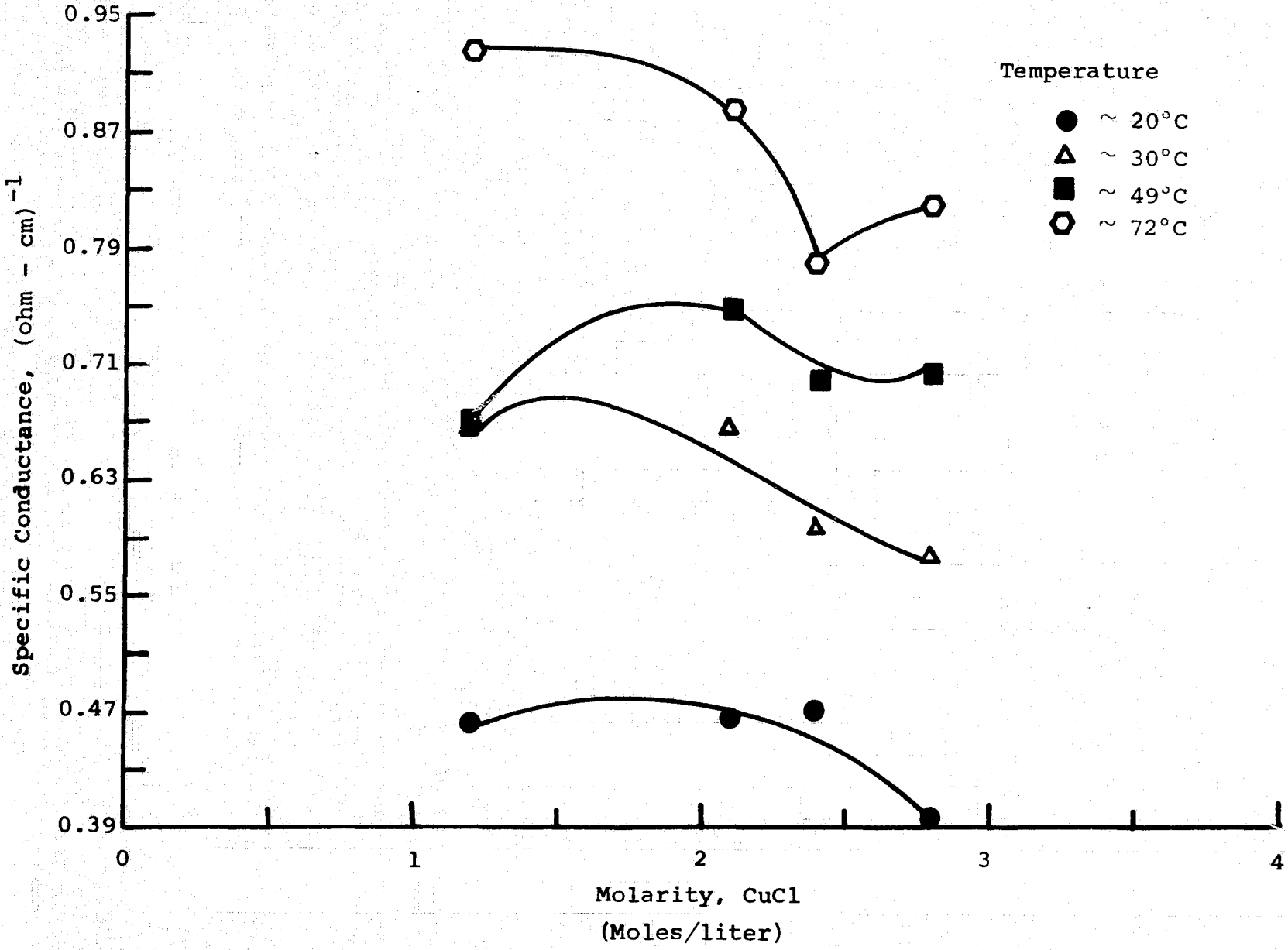

FIGURE 7 : Specific Conductances of the Cuprous Chloride Solutions at Different Temperatures

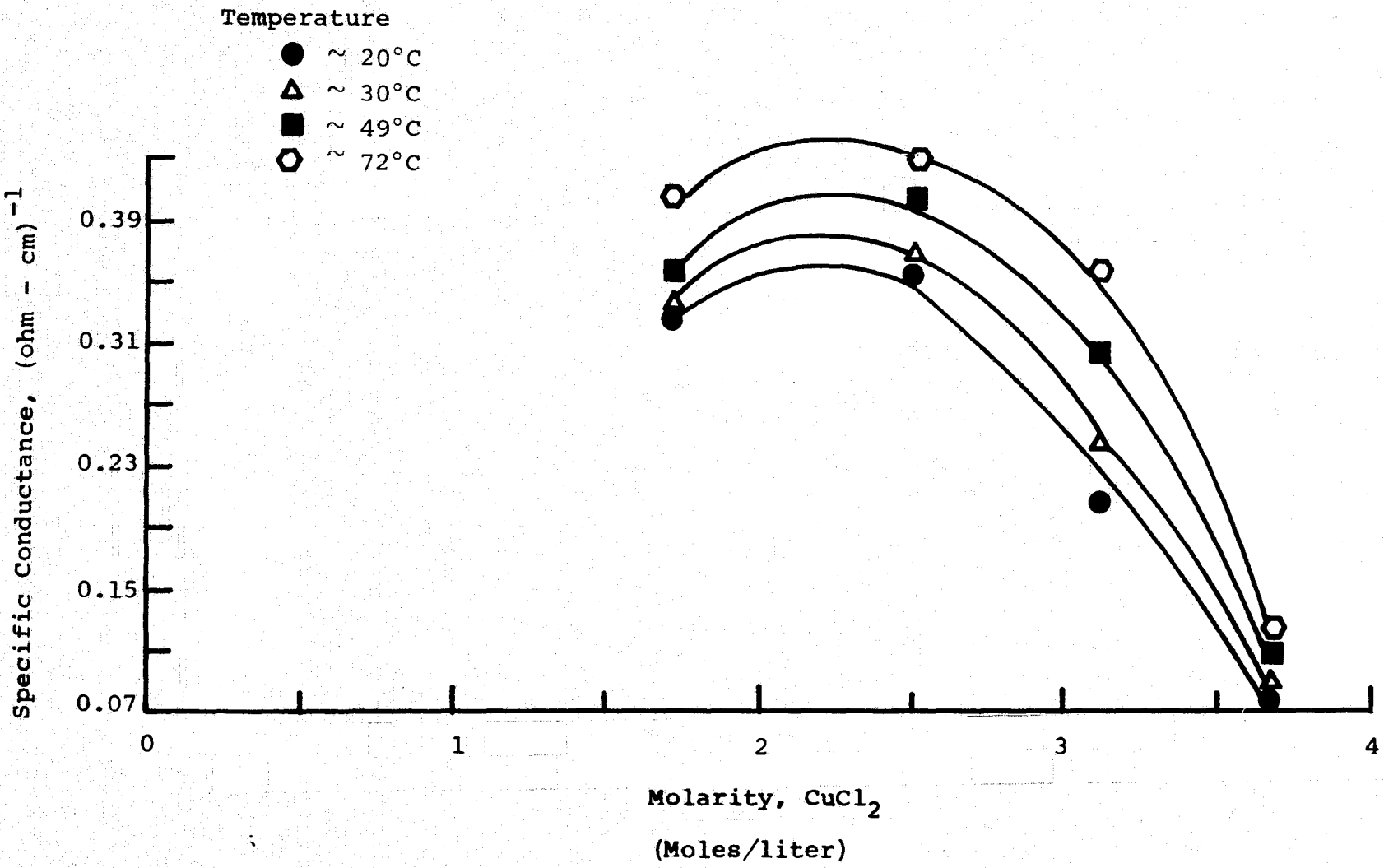

FIGURE 8 : Specific Conductances of the Cupric Chloride Solutions at Different Temperature

(Precision Viscosity Bath, Model S) with the viscometers suspended inside the bath. For each run, 10 ml of the chloride solution was used, and its efflux time (in seconds) was measured.

The kinematic viscosity of the chloride solution (in centistokes) can then be calculated. In this study, the chloride solutions were all saturated solutions. The viscosities of a chloride solution at four different temperatures, namely, 20, 30, 50 and 70°C were measured. Figures 9-12 represent the viscosity respectively of $FeCl_2$, $FeCl_3$, CuCl and $CuCl_2$. For each solution, the viscosity increases as the concentration increases. On the other hand, the viscosity decreases as the temperature increases. Both observations are reasonable.

For titanous chloride, the viscosities of the 20 wt% solution at different temperatures are presented in Table 2.

TABLE 2

KINEMATIC VISCOSITIES OF A 20 WT%
TITANOUS CHLORIDE SOLUTION AT DIFFERENT TEMPERATURES

Temperature °C	22.2	29.9	48.9	71.7
Viscosity Centistokes	3.10	2.74	1.77	1.23

4. Density

The density of the chloride solution was directly measured using a Troemner specific gravity chain balance, (Fisher Scientific Catalog No. 2-167). The gravity chain balance utilizes both plummet displacement principle and the chain weight system for weighing. For liquid system, no calculation is needed, and direct reading from the balance can be used. For each run, 40 ml of the solution was required.

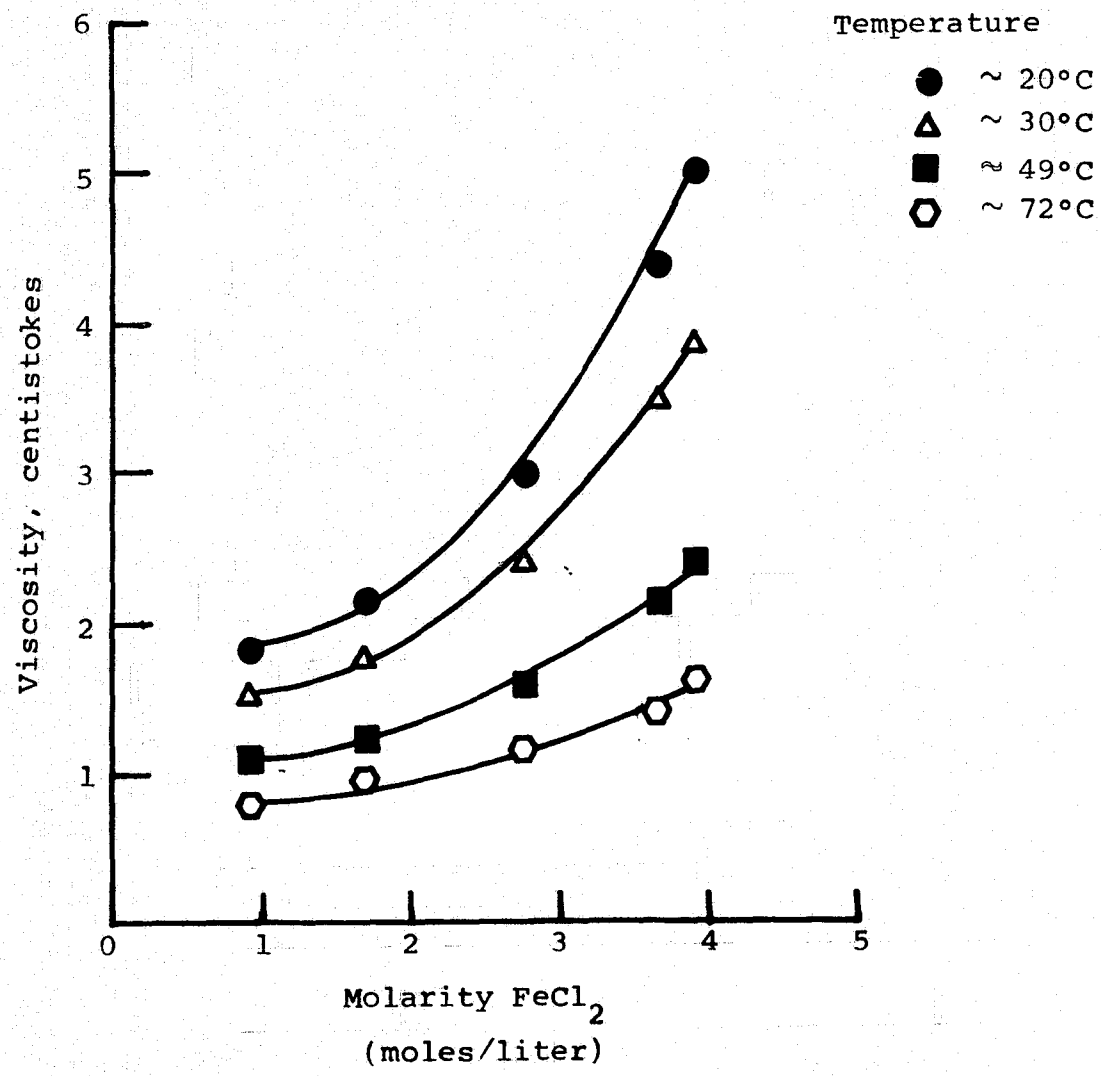

FIGURE 9: Viscosities of the Ferrous Chloride Solutions at Different Temperatures

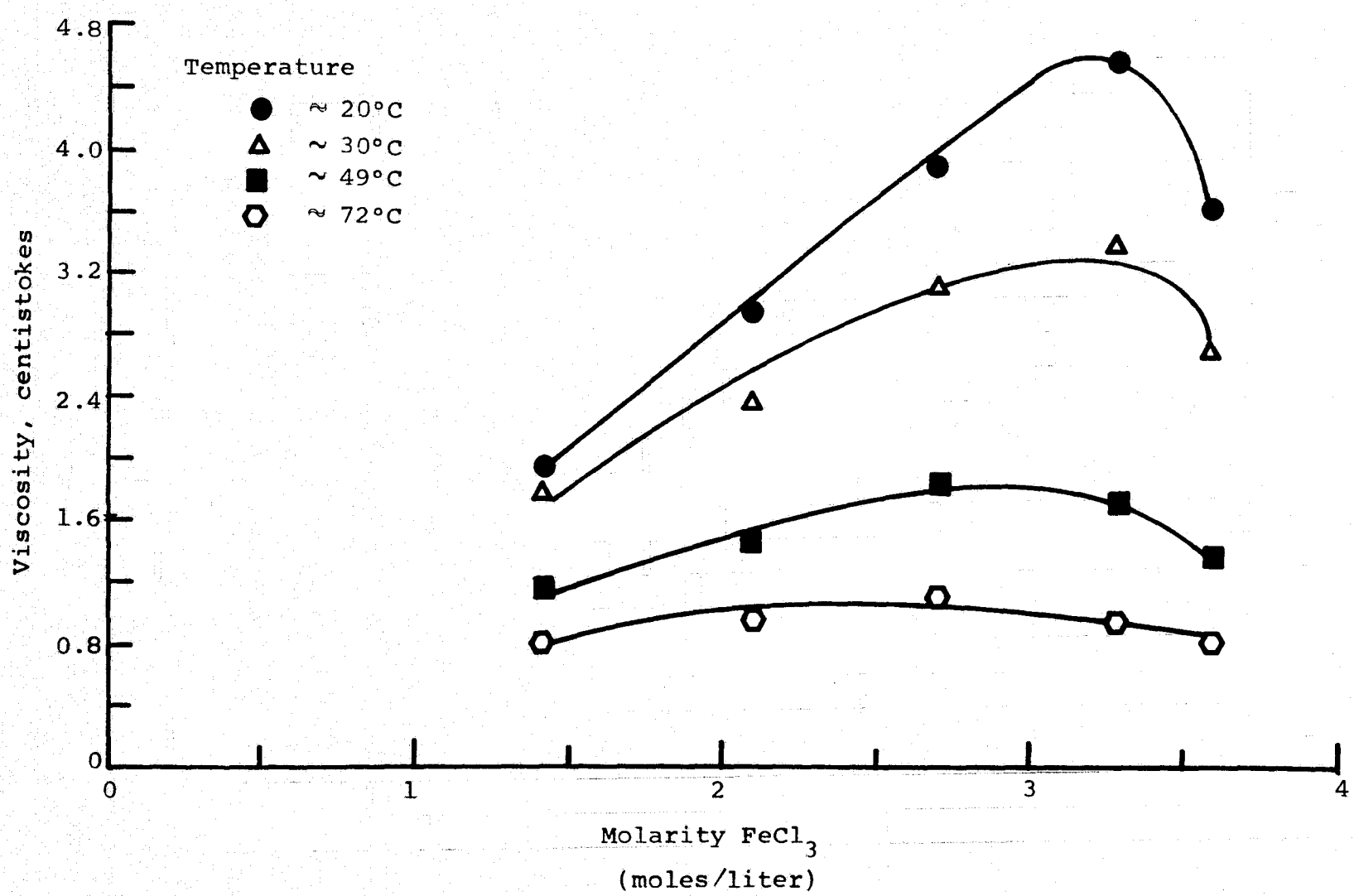

FIGURE 10 : Viscosities of the Ferric Chloride Solutions at Different Temperatures

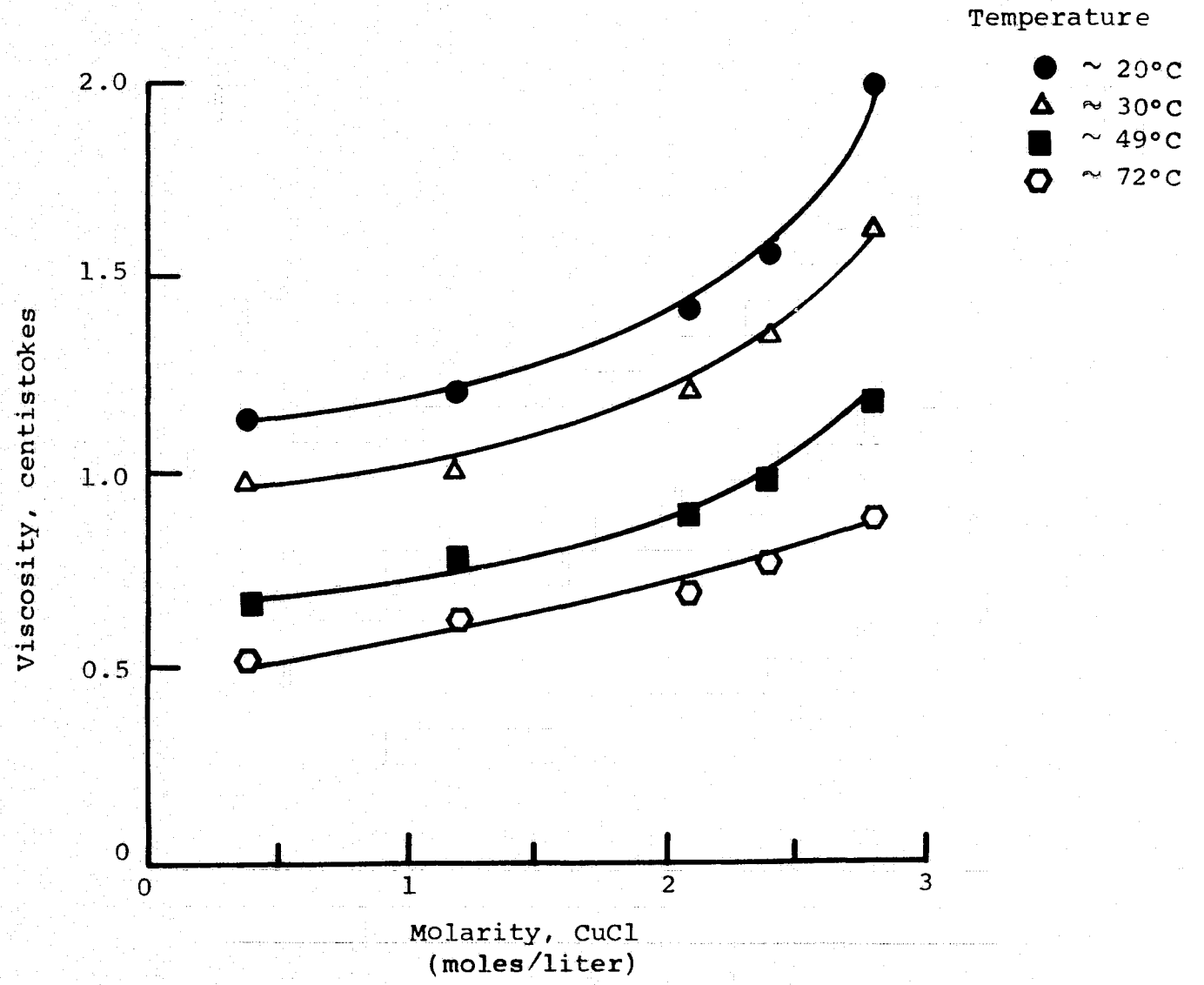

FIGURE 11: Viscosities of the Cuprous Chloride Solutions at Different Temperatures

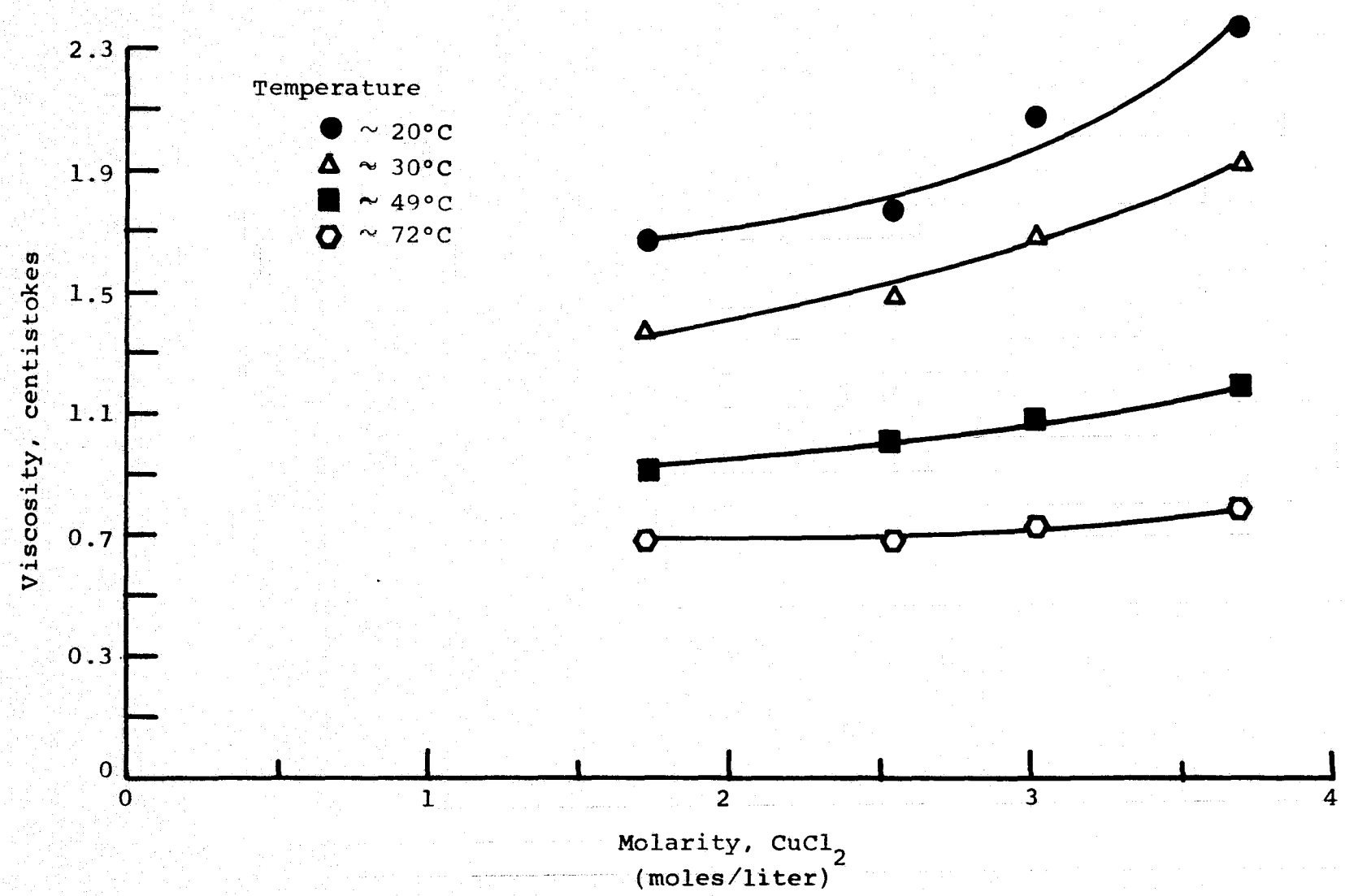

FIGURE 12 : Viscosities of the Cupric Chlorides Solutions at Different Temperatures

Distilled water was used as a standard to calibrate the balance prior to any measurement. The chloride solutions were all saturated solutions prepared as described above. The density of each solution was measured at four different temperatures. The saturated solutions prepared were placed in a capped bottle and suspended inside a constant temperature water bath for at least eight hours. Whenever the density of the solution was measured, 40 ml of this preheated solution was then transferred into the solution holder of the balance for measurement. Heat dissipation may occur during the measurement, but the measurement usually was completed within 20 seconds, and any temperature drop due to the heat loss was considered negligible.

Figures 13-16 represent the density of $FeCl_2$, $FeCl_3$, CuCl and $CuCl_2$ respectively. For each chloride solution the density increases as the temperature decreases. Also a chloride solution of higher molarity has a higher density value. These observations are logical.

For titanous chloride, the densities of a 20 wt% solution at different temperatures are presented in Table 3.

TABLE 3

DENSITIES OF A 20 WT% TITANOUS CHLORIDE SOLUTION AT DIFFERENT TEMPERATURES

Temperature °C	22.3	29.9	48.9	71.7
Density gm/ml	1.218	1.216	1.210	1.206

5. Surface Tension

The surface tension of the chloride solution was measured using a tensiometer (Model 21, Fisher Tensiomat). This tensiometer employs a reversible synchromous motor to raise

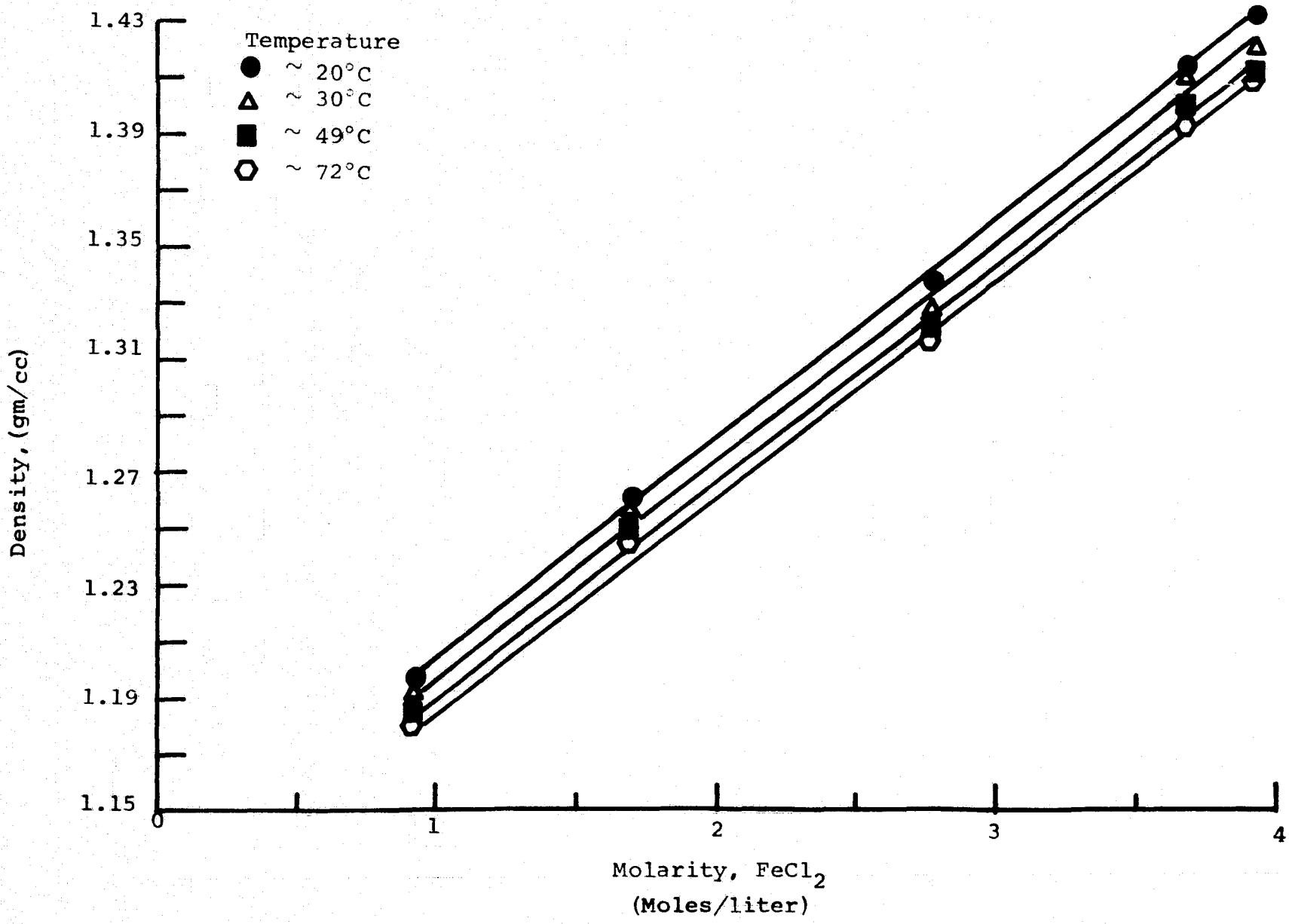

FIGURE 13: Densities of the Ferrous Chloride Solutions at Different Temperatures

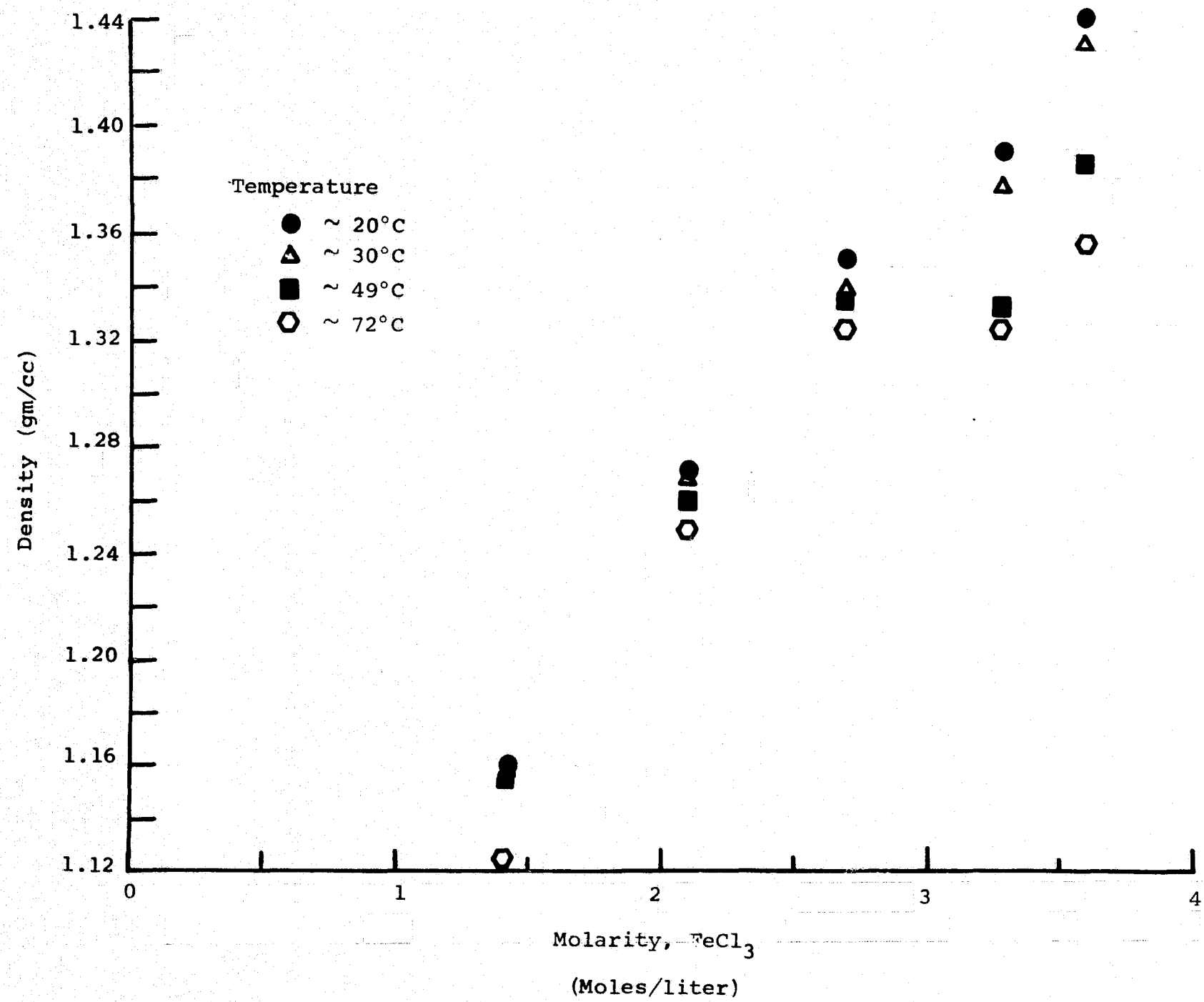

FIGURE 14: Densities of the Ferric Chloride Solutions at Different Temperatures

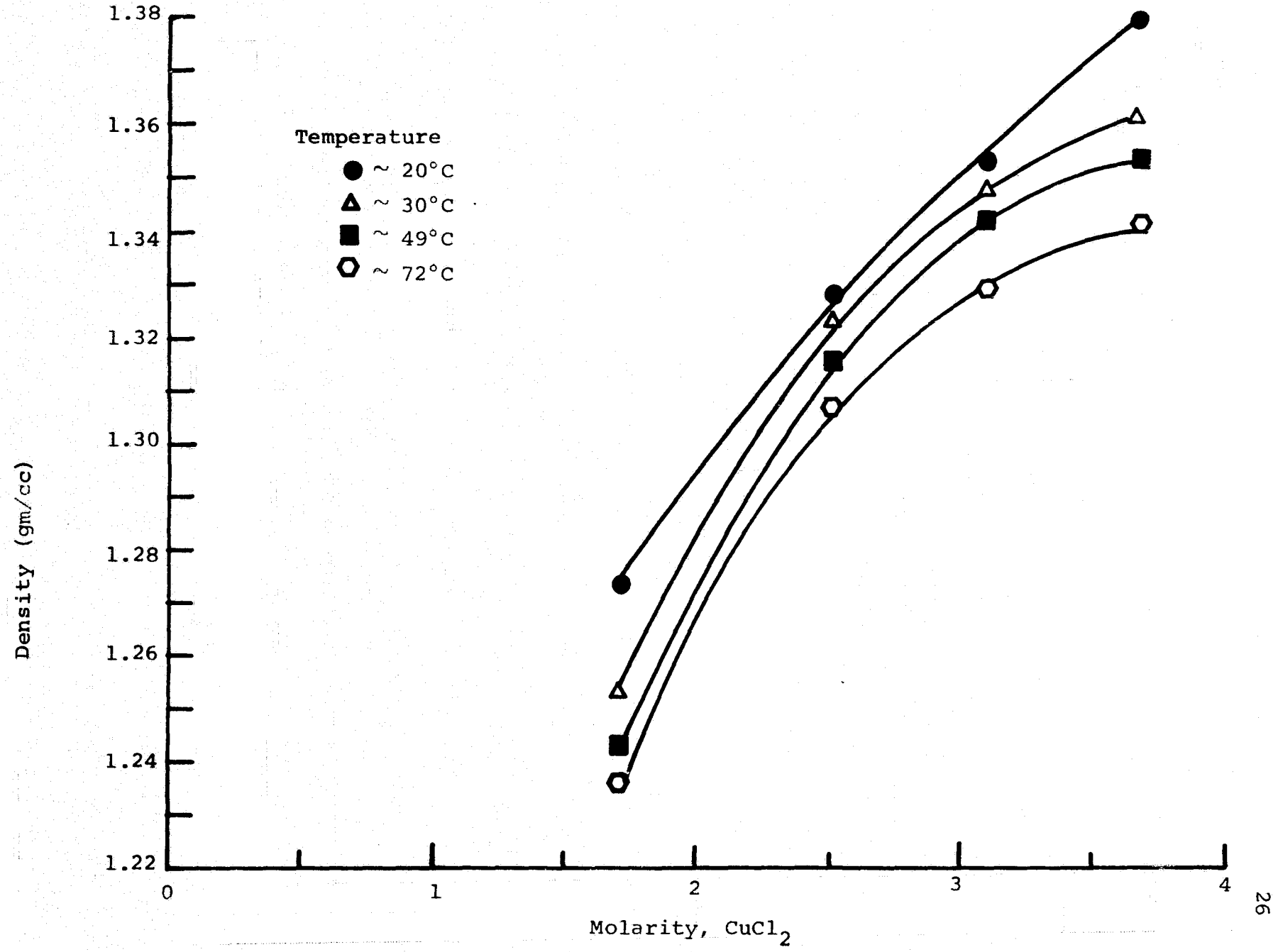

FIGURE 15: Densities of the Cupric Chloride Solutions at Different Temperatures

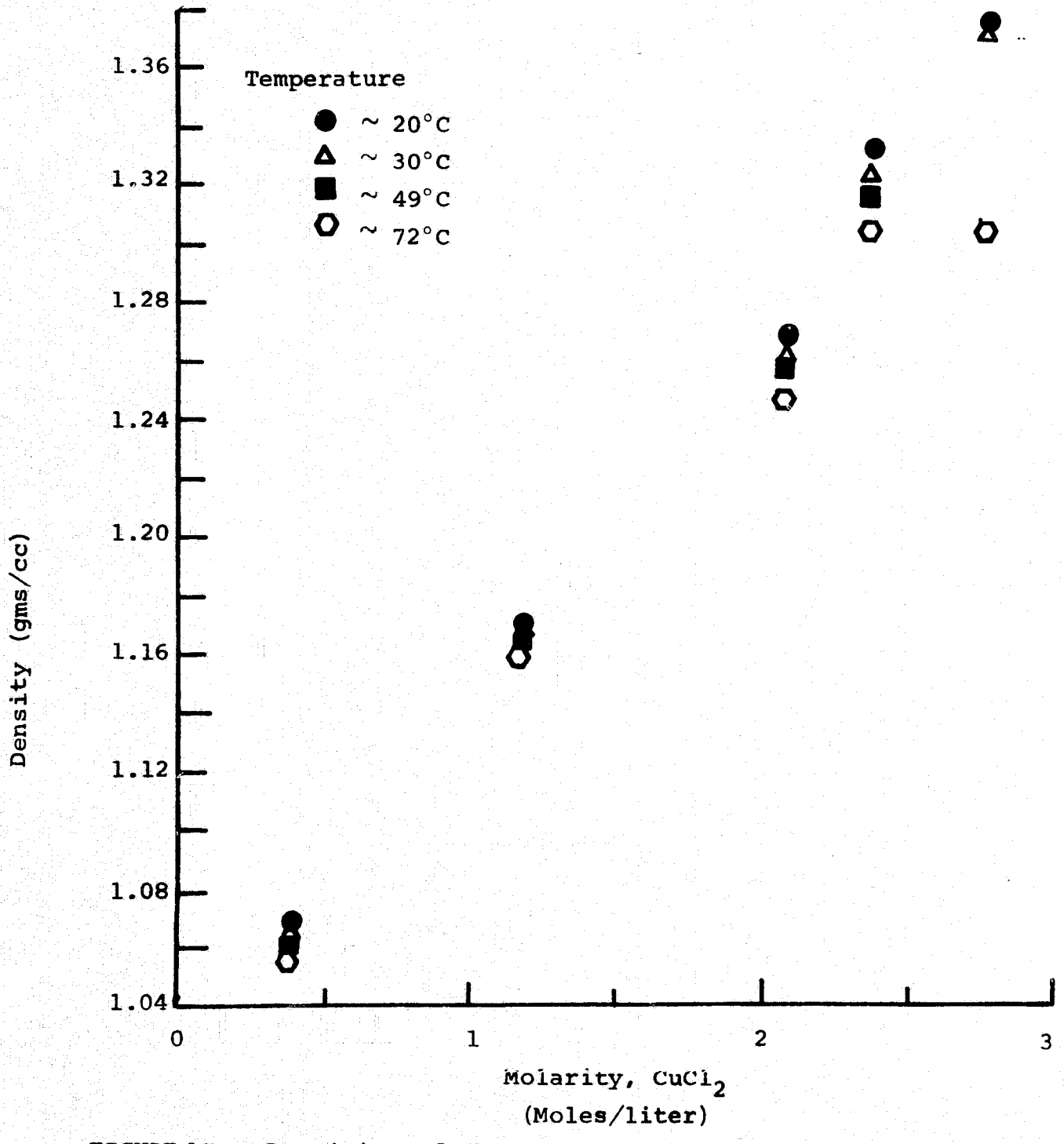

FIGURE 16 : Densities of the cuprous Chloride Solutions at Different Temperatures

or lower the testing ring (platinum-iridum ring, 7 mil in wire diameter and 6.030 cm in circumference) at a uniform rate. When the ring breaks the surface film, a support arm touches a contact and a relay immediately stops the motor. The apparent surface tension (in dyne/cm) is directly obtained. For each run, 150 ml of the chloride solution was used. Similar to the density measurement described above, the saturated chloride solutions were preheated in constant temperature baths. The measurement of the surface tension required approximately 20 seconds, and any heat loss during this period was considered negligible. Figures 17-19 represents the surface tension for $FeCl_2$, $FeCl_3$ and CuCl. $CuCl_2$ were incomplete, at present, and will be reported later. There appears to be no general trend of the surface tension with respect to the molarity of the chloride. For titanous chloride, the surface tension for a 20 wt% solution can be shown in Table 4.

TABLE 4

APPARENT SURFACE TENSION FOR A 20 WT% TITANOUS CHLORIDE SOLUTION

Temperature °C	22.3	29.9	48.9	71.7
Apparent Surface Tension Dyne/cm	67.9	64.8	60.6	59.2

6. Boiling Temperature and Freezing Temperature

Both boiling and freezing temperatures of each chloride solution were measured. Both measurements could be done relatively easily, and were performed under normal 1 atmospheric pressure. For each measurement, 40 ml of the solution was used. For boiling point measurement, direct heating was

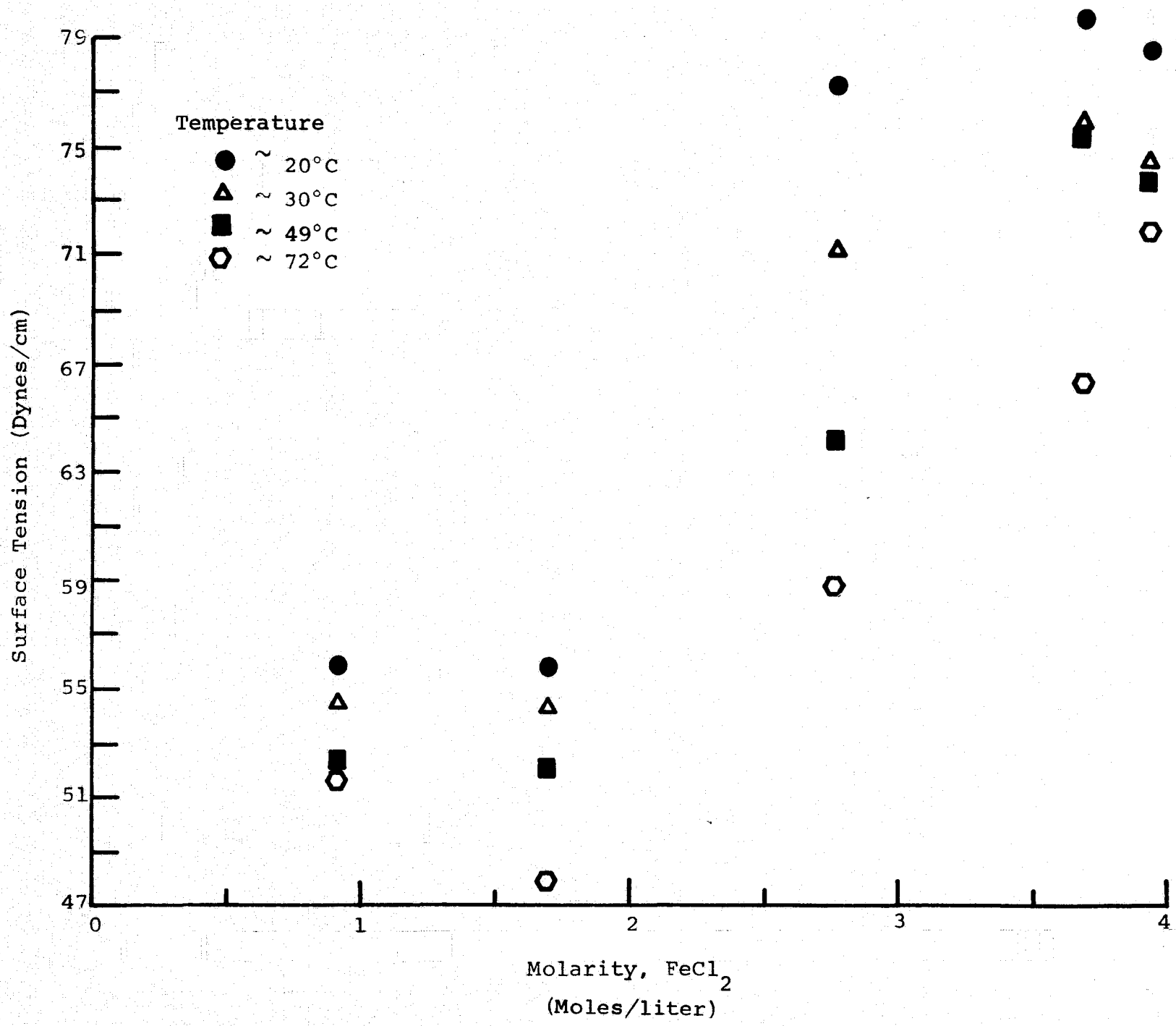

FIGURE 17: Surface Tensions of the Ferrious Chloride Solutions at Different Temperatures

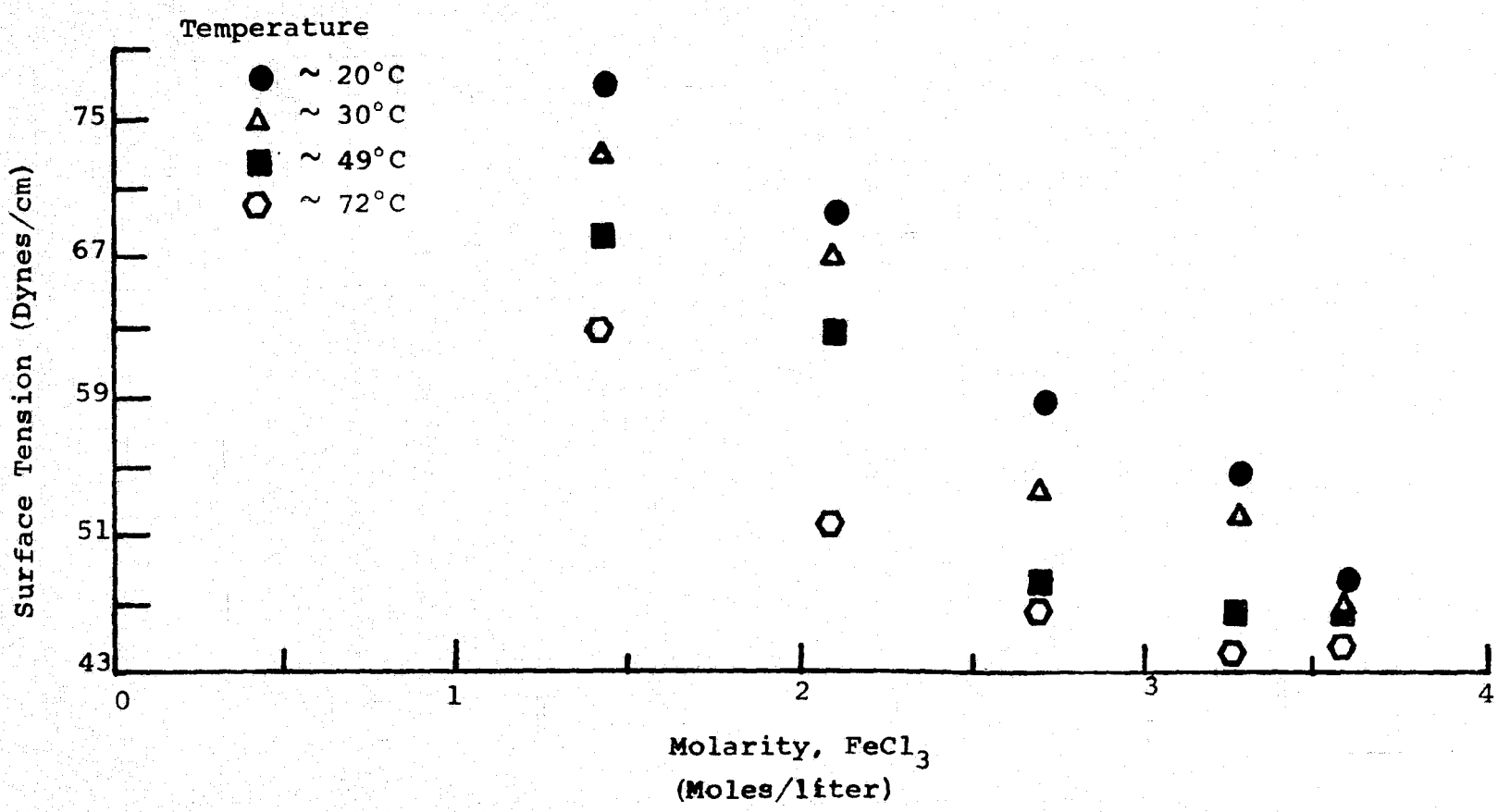

FIGURE 18: Surface Tensions of the Ferric Chloride Solutions at Different Temperatures

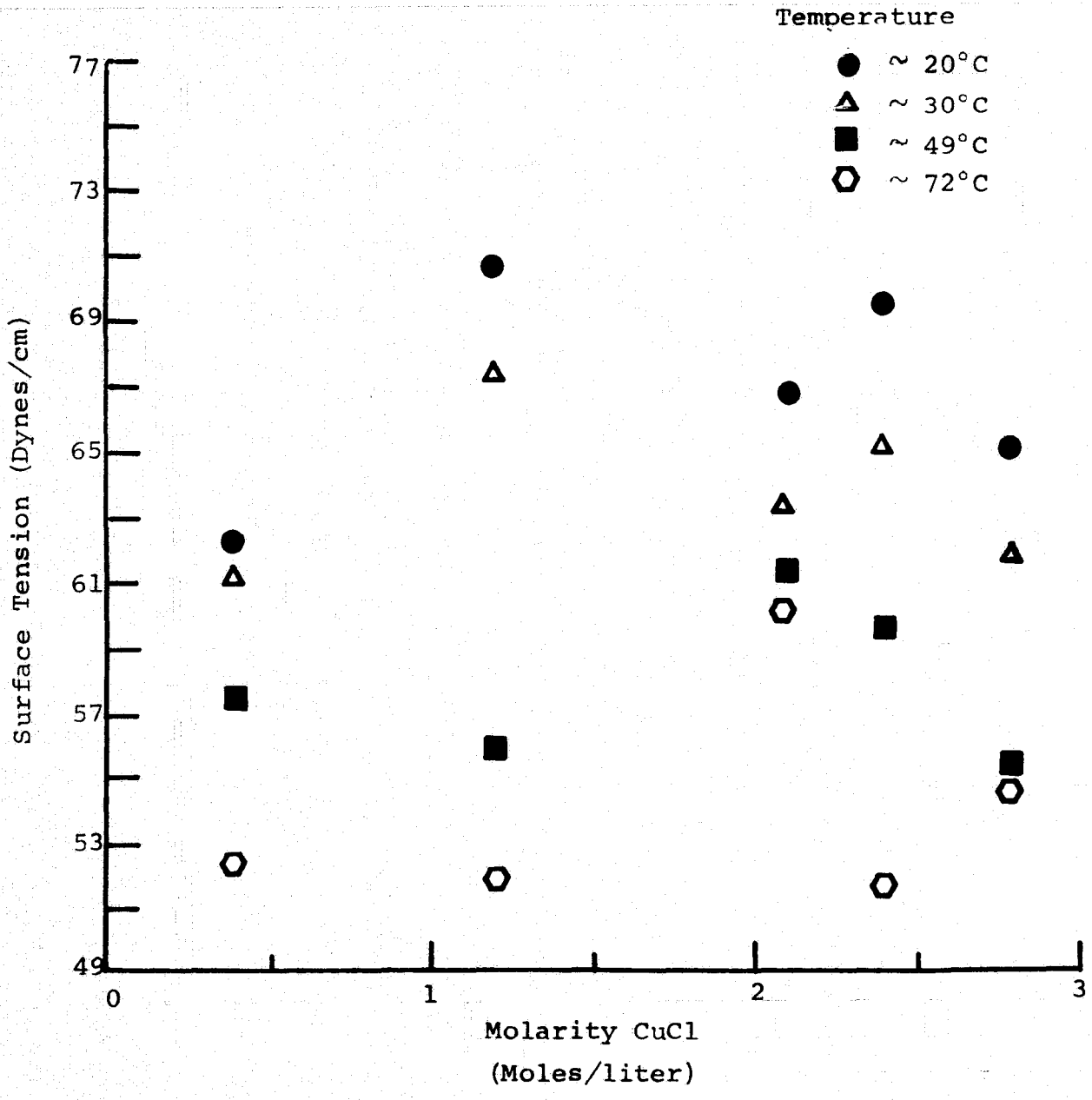

FIGURE 19 : Surface Tensions of the Cuprous Chloride Solutions at Different Temperature

employed, and thermometer was used to measure the temperature. For freezing temperature, a temperature regulatable freezer was employed, and the solution was placed inside the freezer, thermometer was placed inside the solution. The temperature of the freezer was regulated gradually, until the solution appeared to be frozen. For the solutions studied, $FeCl_2$ solution has a boiling temperature of 105.8-108.4°C, freezing temperature of -16.5 - - 19.1°C varying slightly over the molarity range studied. For $FeCl_3$ solution, the boiling point is 103-110°C freezing temperature is ~ -31°C, which also varies over the molarity range of the solution studied. For CuCl solution, the boiling temperature is 104-106°C and boiling temperature for $CuCl_2$ is 106-110°C. The freezing temperatures of these had not been measured.

In summary, this presentation represents the majority of the physical properties of the chloride solutions of interest which are of importance in the development of redox coupled secondary battery systems. Experimental work is time-consuming and required careful preparation. This is most evident in the determination of the solubilities of the chlorides.

Experimental Evaluation of Anion Membranes as the Separator of the Studying Battery Systems

Another important requirement for the redox coupled secondary battery system is the separator. Conventional half-cell separators are made from highly porous and wettable materials. For the developing redox coupled system, ideally, a separator should offer no resistance to the diffusion of the anions, while permitting none of the cations to diffuse through. However, none of the known anion membranes perform ideally. A method is needed to screen prospective anion membranes on the basis of these requirements.

In this phase of study, the method for testing a membrane for the diffusion rate of the cations was developed. For an oxidation reaction of a species, R^{+n},

$$R^{+n} \rightleftarrows P^{+n+Z} + Ze^{-} \qquad (1)$$

The Nernst Equation can then be expressed as

$$E_j = E_{jo} - \frac{RT}{Z_j F} \ln \left[\frac{a_p}{a_r}\right] \qquad (2)$$

where E_j is the half-cell potential and E_{jo} is the standard half-cell potential. The nomenclatures of R, T, Z_j, F and a have the general thermodynamic meanings. For a galvanic cell at a fixed temperature, with the same reactants and products present in both half-cells, the measured potential of the overall cell, E_c, is

$$E_c = E_1 - E_2 = \frac{RT}{ZF} \ln \left[\frac{a_{p2} a_{r1}}{a_{r2} a_{p1}}\right] \qquad (3)$$

in which the subscripts 1 and 2 represent the two half-cells.

For activity $a = \gamma C$ where γ is the activity coefficient and C its constant, Equation (3) becomes

$$E_c = \frac{RT}{ZF} \ln \left[\frac{\gamma_{a1}\ \gamma_{b2}\ C_{a1}\ C_{b2}}{\gamma_{a2}\ \gamma_{b1}\ C_{a2}\ C_{b1}} \right]^{*} \qquad (4)$$

If the activity coefficients are the same order of magnitude and the concentration of the reactant C_b in both half-cells is identical, then Equation (4) can be approximated by

$$E_c = \frac{RT}{ZF} \ln \left[\frac{C_{a1}}{C_{a2}} \right] \qquad (5)$$

From Equation (5) the measured cell potential can be used to interpret the ratio of the concentrations of component a in half-cell 1 and 2. If we know the concentration of component a in half-cell 1 at a specific time, based on the cell potential measurements at that time, the concentration of a in half-cell 2 can be calculated. This information can then be used to obtain the diffusion rate of component a through the anion membrane (the separator).

Thus, the reaction takes place only with an accompanying transfer of electrons, therefore, if there is no current flow, then a mass balance of a specific cations, at any given time, can be written as

$$C_{a1} + C_{a2} = C_{a1}^{\circ} + C_{a2}^{\circ} \qquad (6)$$

---

*For the purpose of generality, r and p are replaced by a and b, respectively.

The superscripts (o) refer to the initial concentration of the cations, and the volumes of the two half-cells are assumed to be equal and unchanging. Solving Equations (5) and (6), simultaneously for E_c in terms of C_{a2}, C_{a1}^{o}, and C_{a2}^{o}, one obtains

$$E_c = \frac{RT}{FZ} \ln \left[\frac{C_{a2}}{C_{a1}^{o} + C_{a2}^{o} - C_{a2}} \right] \qquad (7)$$

Consequently, by rearranging this equation, one obtains

$$C_{a2} = \frac{(C_{a1}^{o} + C_{a2}^{o}) e^{\frac{E_c FZ^*}{RT}}}{\left(1 + e^{\frac{E_c FZ}{RT}}\right)} \qquad (8)$$

In this equation, C_{a2} is the cation concentration in the half-cell with the lower initial concentration, which means, from Equation (5), that E_c will always be negative. Equation (8) is then used to convert cell potential measurements, E_c, to the concentration of the cations on the lower concentration side, C_{a2}.

For practical purposes, a polynomial regression analysis technique is applied to obtain C_{a2} as a function of time in the form of

$$C_{a2} = \sum_{i=o}^{4} f_i t^i \qquad (9)$$

---

*For experimental convenience, one may take the absolute value of $|E_c|$ and add a minus sign expressing it as $-|E_c|$.

where the f's are statistically determined coefficients. If Fick's First Law for constant density diffusion is applicable, then

$$D_a = \frac{-J_a}{\frac{dC_{aj}}{dx}} \qquad (10)$$

where D_a is the diffusion coefficient of the a cations. Using the volume of the half-cell, V, and the area of the membrane, A, the flux may be written as

$$J_a = \frac{dC_{a2}}{dt}\frac{V}{A} \qquad (11)$$

The cation concentration gradient in each half-cell is assumed to be zero at all times, and the concentration gradient across the membrane is assumed to be linear. The diffusion coefficient for species a is obtained by eliminating J_a from Equations (10) and (11) and integrating C_{aj} over the thickness of the membrane L. Then the diffusion coefficient for species a can be expressed as

$$D_a = -\frac{\frac{dC_{a2}}{dt} VL}{A\,(C_{a2} - C_{a1})} \qquad (12)$$

This can be modified by substituting Equation (6) for C_{a1}, Equation (9) for C_{a2}, and performing the indicated differentiation. Thus, the diffusion coefficient for species a can be expressed as

$$D_a = \frac{VL \sum_{i=o}^{4} i f_i t^{i-1}}{A(C_{a2}^{o} + C_{a1}^{o} - 2 \sum_{i=o}^{4} f_i t_i)} \qquad (13)$$

This equation is used to evaluate the diffusion coefficient of the cations through the membrane. In this study, six different anion membranes were tested for the diffusion rate of cations through them. The anion membranes tested were the Ionac Corporation's (Birmingham, New Jersey) IM-12 and 3475 membranes; the Ionic Corporation's (Watertown, Massachusetts) 111BZL-183, 111BZL-65, 111BZL-66 membranes (hereafter referred to as 183, 065, and 066 respectively); and Asahi Glass Corporation's (Tokyo, Japan) AMV anion membrane.

Of the ten cations used in the theoretical analysis, eight (Ti^{+3}, Ti^{+4}, Cr^{+2}, Cu^{+3}, Sn^{+2}, Sn^{+4}, Fe^{+3}) were used. The other two (Cu^{+1} and Cu^{+2}) were not considered in the experimental work because the theoretical analysis indicated that these ions were relatively impractical in this development.

The concentration cell was made of 5.08 centimeter inside diameter plexiglass tube with a wall thickness of .636 centimeters. The cell is made of two symmetric halves, each half 5.08 centimeters long. The concentration cell was then suspended in a constant temperature bath.

Throughout this study, each cell was run for at least 85 hours. The initial concentration of the reactant in the half-cell were 0.1 molar on the high concentration side and 0 molar on the other. The reactant and prcduct solutions were made with distilled water with 12N HCl added, when needed,

to assure a complete dissolution of the chloride salts. The water in each half-cell was deoxygenated for at least 15 minutes using 99.9% pure nitrogen gas. The apparent Fick's Law diffusion coefficients were obtained for each cation at 310°K and are summarized in Table 5. In principle, the lower the apparent Fick's Law diffusion coefficient, the better the membrane was for this application.

In general, for all the membranes studied, the diffusion coefficients for the lower valence ions were higher than those of the higher valence ions. This is an expected result as the number of water molecules associated with the higher valence ions are greater than the number associated with the lower valence ions. The greater the number of water molecules, the larger the ion-water complex, and the lower the diffusion coefficient becomes. The magnitudes of the apparent coefficients for cation diffusion through these anion membranes range from two to twenty orders of magnitude greater than those of the cations in aqueous solutions.

Table 5 illustrates the effect of the thickness of the anion membrane on the diffusion rate of the cations through the membrane. The thickest membrane (065, which was .120 centimeters thick), had a higher diffusion rate for most of the cations than the thinnest (AMV, .011 centimeters thick) membrane. This observation is true even for membranes made by the same company. This unexpected result might be explained by the following postulation. There are two contributions to the thickness of these membranes. One is the thickness of the actual anion selective component. The other is the thickness of supporting material, increasing the resistance of the membrane to pressure. Therefore, the total thickness of a membrane is not necessarily an indication of

the thickness of the anion selective component per se. Since the thickness of the anion selective component for each membrane is unknown, no definite conclusion can be drawn. However, we would expect that as the thickness of the anion selective component is increased, the diffusion of the cations through the anion membranes would be decreased.

Of the six anion membranes tested, the Asahi Glass AMV anion membrane generally had the lowest cation diffusion rates. The apparent diffusion coefficients of the cations tended to be directly related to the perm-selectivity or transference number provided by the manufacturers. In general, the higher the claimed perm-selectivity or transference number of the anion membrane for the chloride anions, the lower the diffusion coefficient for the cations observed. The perm-selectivities were 85% for the 185, 065, and 066 membranes, 87% for the IM-12 membrane, and 92% for the 3475 membrane. The transference number for the AMV membrane was about .96 for the Cl^- anions. In this respect, the Asahi Glass AMV anion membrane had the highest transference number and generally the lowest diffusion coefficient, thus substantiating the above observation.

Table 6 presents the apparent Fick's Law diffusion coefficients of the cations for two anion membranes (IM-12 and 3475) at three different temperatures (310°K, 330°K, and 350°K). As expected, the diffusion coefficient generally increases with increasing temperature.

TABLE 5

EXPERIMENTAL DIFFUSION COEFFICIENTS FOR VARIOUS CATIONS AT 310°K

Cation \ Membrane	IM-12	3475	183	065	066	AMV
Ti^{+3}	12.1*	9.29	9.77	6.63	7.47	9.98
Ti^{+4}	>13.0	10.1	8.53	7.52	10.5	>13.0
Cr^{+2}	10.3	9.33	7.79	6.64	6.79	11.2
Cr^{+3}	8.81	7.72	8.78	10.8	7.17	11.5
Sn^{+2}	9.32	9.84	7.94	6.63	7.71	11.7
Sn^{+4}	6.86	7.02	9.05	7.66	12.3	>13.0
Fe^{+2}	9.16	7.35	7.47	8.69	7.26	8.33
Fe^{+3}	>13.0	6.54	9.77	>13.0	7.63	>13.0

*Negative base ten logarithms of the experimentally obtained diffusion coefficients are presented. The units on the original diffusion coefficients were centimeters squared per second.

TABLE 6

Experimental Diffusion Coefficients for Various Cations at 310°K, 330°K, and 350°K

Cations \ Membrane	310°K		330°K		350°K	
	IM-12	3475	IM-12	3475	IM-12	3475
Ti^{+3}	12.1*	9.29	10.3	6.67	7.59	6.35
Ti^{+4}	> 13.0	10.1	7.85	6.29	10.61	6.17
Cr^{+2}	10.3	9.33	> 13.0	6.93	8.27	6.97
Cr^{+3}	8.81	7.72	8.67	8.26	8.57	7.24
Sn^{+2}	9.32	9.84	8.79	8.12	7.29	6.59
Sn^{+4}	6.86	7.02	7.69	8.34	7.38	6.89
Fe^{+2}	9.16	7.35	6.85	7.10	7.27	7.00
Fe^{+3}	> 13.0	6.54	6.84	7.92	7.34	6.89

*The negative base ten logarithms of the experimentally obtained diffusion coefficients are presented. The units on the original diffusion coefficients were centimeters squared per second.

Evaluation of the Battery Performance of the Prototype Secondary Battery Systems

Even though the principle of this redox secondary battery system is attractive, the practical performance of this battery system has not been tested. Thus, in this phase of research, prototype of this redox secondary battery system was constructed and evaluated. Over the 12-months period of time, the following studies have been made:

(1) Design fabrication of a prototype testing cell

(2) Development of computer-controlled testing facilities and required software, and

(3) Evaluation of the battery-operation characteristics of the testing systems.

The prototype testing unit was made with lucite, and is shown in Figure 20. It had a compartmental diameter of 5 cm and a depth of 1 cm. The anion membrane was mounted between the two half-cells and held in place by gaskets. The electrodes used here was a conductive graphite felt (Union Carbide, VDL-X3530) placed next to the membrane. A platinum screen in the size of $\sim$ 1 cm^2 was placed in the middle of the graphite felts. The platinum screen was then connected to the lead wires which were platinum wires of 3 mil diameter in this case. The lead wires were then connected to the switching control system.

In this study, a Hewlett-Packard 2114B minicomputer was employed. It serves two basic functions in this work: (1) automatically control the experimental condition and (2) monitor and record experimental data. In the first function, the computer was programmed to switch the external loads and the power supplier for charging of the testing cells. We have constructed a relay box which consisted of three different

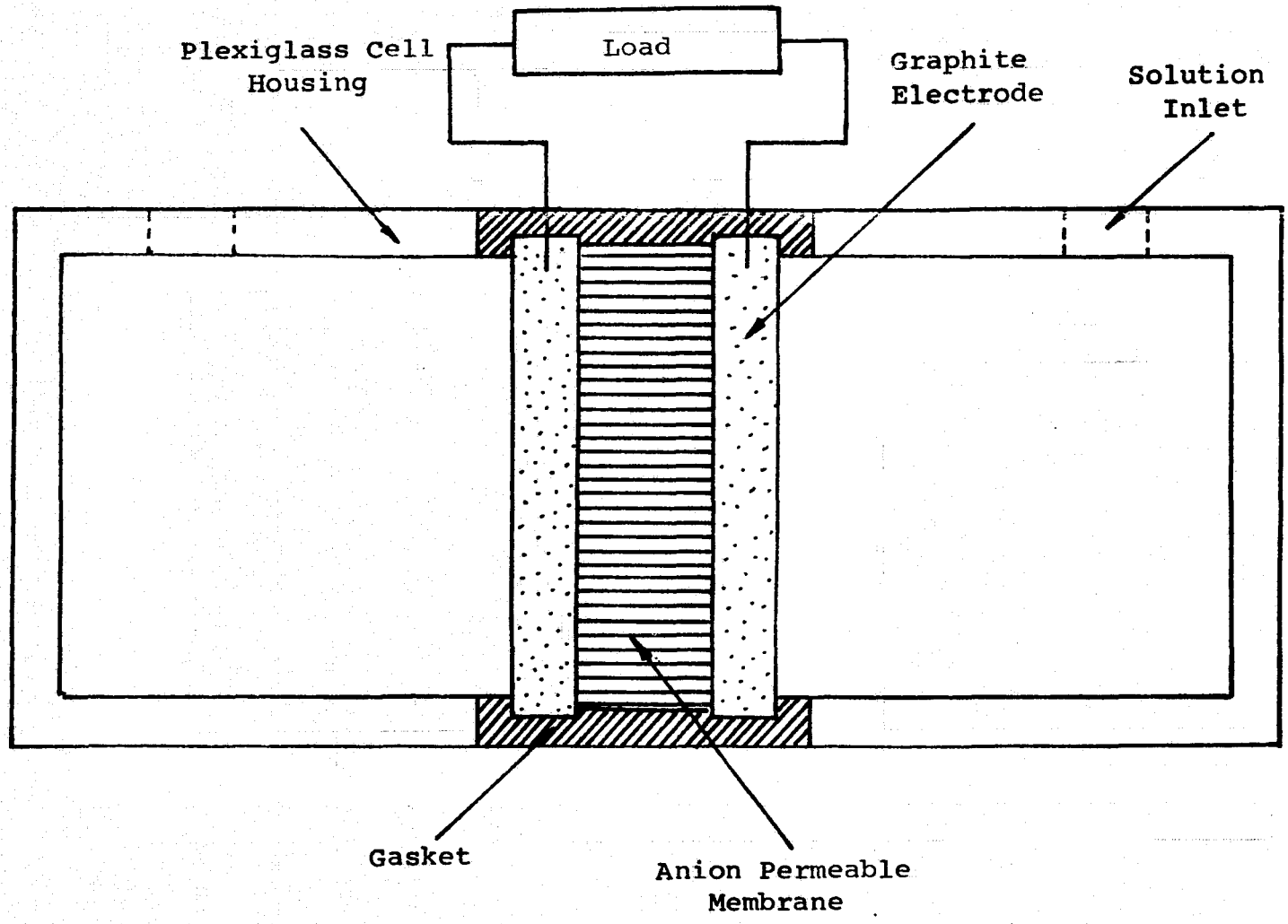

FIGURE 20: Schematic Structure of the Prototype Testing Cell Unit

loads (resistors) of 10 ohms, 100 ohms and 1000 ohms and connected this apparatus to a constant voltage power supplier. At a predetermined time, the computer would activate the proper contacts. Consequently, the testing cell would be in an operating mode of 10 ohm load, 100 ohm load, 1000 ohm load or being charged. In the second function, the potential of the cell under load was measured and the data was recorded. Both operational steps were done by the computer at a predetermined time period. Normally, the computer would record and store the data every 100 seconds. The data could be retrieved and printed on teletype when necessary. This data could be presented in the form of actual recording potential as a function of time or in a polynomial expression or both. If desired, the data could be punched out on paper type which could then be used with a larger computer. The University of Pittsburgh maintains a PDP-10 system which was used in this study.

In this study, the following experimental data from the testing cells were monitored:

(1) discharge potential as a function of time under the actual load condition.

(2) charge potential and current as a function of time under the actual load conditions.

(3) energy efficiency of the testing cells.

(4) cycle life and cyclic battery-operating characteristics of the testing cells, and

(5) probability of the battery failure as a function of time and conditions of use.

Experimental parameters in the systems includes the reactant concentrations, types of membrane, lengths and methods of charge cycles etc. Studies of these redox battery systems

were very extensive so we can report only partial results of our continuous, ongoing investigation. The following tables reported the redox couple systems studied thus far.

TABLE 7

Experimental Results for the Iron-Titanium Redox Couple Prototype Cell

Concentration (moles/liter)	1	1	1	1	1	1	1
Temperature (°K)	310	310	310	310	330	330	330
Membrane Area (square centimeters)	19.6	19.6	19.6	19.6	19.6	19.6	19.6
Membrane	IM-12	IM-12	IM-12	183	3475	3475	3475
Discharge Time (hours)	6	6	6	6	4	8	8
Maximum Cell Potential (volts)	.70	.70	.70	.70	.80	.80	.80
% Energy Efficiency	90+	90+	90+	90+	40.8	28.1	5.15
% Power Efficiency	17.8	1.78	1.83	59.3	----	----	20.4
% Energy Remaining in Cell	65.0	55.9	64.8	39.2	64.2	0	15.0
External Load Resistance (ohms)	10	100	1000	100	10	10	100
Current Density x 10^{+3} (amperes/square centimeter)	3.60	.360	.0360	.333	1.66	.797	.203
Run Number	231	233	235	263	081	091	093

TABLE 7
(Concluded)

Concentration (moles/liter)	.25	.25	.25	.25	.125	.125	.125
Temperature (°K)	310	310	310	310	310	310	310
Membrane Area (square centimeters)	19.6	19.6	19.6	19.6	19.6	19.6	19.6
Membrane	AMV	AMV	AMV	AMV	AMV	AMV	AMV
Discharge Time (hours)	8	16	16	16	8	16	16
Maximum Cell Potential (volts)	.67	.67	.67	.67	.67	.67	.67
% Energy Efficiency	90+	46.3	90+	90+	90+	37.6	90+
% Power Efficiency	58.5	32.9	16.2	1.60	4.02	28.4	1.86
% Energy Remaining in Cell	46.5	32.7	37.4	61.7	21.7	95.7	61.4
External Load Resistance (ohms)	1000	10	100	1000	1000	10	1000
Current Density x 10^{+3} (amperes/square centimeter)	.342	3.42	.342	.0342	.0342	1.24	.0342
Run Number	483	441	443	445	495	451	455

TABLE 7
(Continued)

Concentration (moles/liter)	1	1	1	1	1	.5	.25
Temperature (°K)	310	310	290	210	310	310	310
Membrane Area (square centimeters)	19.6	19.6	19.6	19.6	19.6	19.6	19.6
Membrane	3475	3475	3475	AMV	AMV	AMV	AMV
Discharge Time (hours)	3	3	6	16	16	16	8
Maximum Cell Potential (volts)	.78	.78	.80	.67	.67	.67	.67
% Energy Efficiency	29.3	55.8	7.79	90+	90+	90+	59.6
% Power Efficiency	----	25.6	----	16.2	14.4	1.74	80.8
% Energy Remaining in Cell	31.9	33.2	0	85.6	42.9	57.4	37.2
External Load Resistance (ohms)	10	100	10	100	1000	1000	10
Current Density x 10^{+3} (amperes/square centimeter)	1.07	.218	.176	.342	.0342	.00342	2.03
Run Number	011	013	101	393	395	435	481

TABLE 8

Experimental Results for the Iron-Tin Redox Couple Prototype Cell

Concentration (moles/liter)	1	1	.5	.5	.25	.25	.25	1
Temperature (°K)	310	310	310	310	310	310	310	310
Membrane Area (square centimeters)	19.6	19.6	19.6	19.6	19.6	19.6	19.6	19.6
Membrane	AMV	AMV	AMV	AMV	AMV	AMV	AMV	AMV
Discharge Time (hours)	16	16	16	16	6	6	6	6
Maximum Cell Potential (volts)	.62	.62	.62	.62	.62	.62	.62	.62
% Energy Efficiency	90+	90+	6.1	90+	54.4	90+	90+	90+
% Power Efficiency	17.3	1.5	.216	3.29	90+	21.3	1.78	90+
% Energy Remaining in Cell	55.3	48.1	0	31.9	35.9	13.8	20.3	17.8
External Load Resistance (ohms)	100	1000	10	1000	10	100	1000	10
Current Density x 10^{+3} (amperes/square centimeter)	.316	.0316	.0194	.0316	1.71	.317	.0317	3.15
Run Number	373	375	411	415	351	353	355	241

TABLE 9

Experimental Results for the Tin-Chromium Redox Couple Prototype Cell

Concentration (moles/liter)	1	1	.5	.5	.25	.25	.125	.125	.125
Temperature (°K)	310	310	310	310	310	310	310	310	310
Membrane Area (square centimeters)	19.6	19.6	19.6	19.6	10.75	10.75	5.73	5.73	5.73
Membrane	AMV	AMV	AMV	AMV	AMV	AMV	AMV	AMV	AMV
Discharge Time (hours)	16	16	16	16	16	16	16	8	8
Maximum Cell Potential (volts)	.56	.56	.56	.56	.56	.56	.56	.56	.56
% Energy Efficiency	76.9	90+	90+	90+	69.6	90+	90+	29.8	90+
% Power Efficiency	----	9.69	18.9	1.14	90+	13.7	2.00	35.3	3.81
% Energy Remaining in Cell	1.92	34.8	31.5	46.7	35.1	44.0	11.3	6.65	23.3
External Load Resistance (ohms)	10	100	100	1000	10	100	1000	10	1000
Current Density x 10^{+3} (amperes/square centimeter)	2.16	.286	.286	.0286	3.62	.521	.0547	1.45	.0978
Run Number	381	383	423	425	461	463	475	511	515

TABLE 10

Experimental Results for the Iron-Chromium Redox Couple Prototype Cell

Concentration (moles/liter)	1	.5	.5	1	1	1
Temperature (°K)	310	310	310	350	350	350
Membrane Area (square centimeters)	19.6	19.6	19.6	19.6	19.6	19.6
Membrane	AMV	AMV	AMV	3475	3475	3475
Discharge Time (hours)	16	16	16	2	2	2
Maximum Cell Potential (volts)	1.2	1.2	1.2	1.2	1.2	1.2
% Energy Efficiency	72.7	18.8	90+	15.4	64.2	10.7
% Power Efficiency	42.2	----	3.09	12.5	26.5	.107
% Energy Remaining in Cell	0	30.8	64.3	11.3	23.3	42.8
External Load Resistance (ohms)	1000	10	1000	10	100	1000
Current Density x 10^{+3} (amperes/square centimeter)	.0361	.850	.0611	.903	.385	.00653
Run Number	365	401	405	061	063	065

TABLE 10
(Continued)

Concentration (moles/liter)	1	1	1	1	.5	.5
Temperature (°K)	310	310	310	310	310	310
Membrane Area (square centimeters)	19.6	19.6	19.6	19.6	19.6	19.6
Membrane	IM-12	IM-12	IM-12	065	065	065
Discharge Time (hours)	6	6	6	6	6	6
Maximum Cell Potential (volts)	1.2	1.2	1.2	1.2	1.2	1.2
% Energy Efficiency	22.2	14.9	90+	86.6	39.4	90+
% Power Efficiency	----	16.6	4.18	59.6	53.9	27.2
% Energy Remaining in Cell	0	51.3	80.5	0	86.5	0
External Load Resistance (ohms)	10	1000	100	100	10	100
Current Density x 10^{+3} (amperes/square centimeter)	1.11	.00907	.0612	.382	2.30	.544
Run Number	171	175	225	283	291	293

TABLE 10
(Concluded)

Concentration (moles/liter)	.25	.25	.125	1	1	1
Temperature (°K)	310	310	310	310	310	310
Membrane Area (square centimeters)	19.6	19.6	19.6	19.6	19.6	19.6
Membrane	065	065	065	183	183	183
Discharge Time (hours)	6	6	6	6	6	6
Maximum Cell Potential (volts)	1.2	1.2	1.2	1.2	1.2	1.2
% Energy Efficiency	10+	90+	90+	90+	90+	90+
% Power Efficiency	30.2	2.95	2.98	24.1	36.4	3.23
% Energy Remaining in Cell	95.2	19.7	0	31.2	39.0	66.7
External Load Resistance (ohms)	100	1000	1000	100	100	1000
Current Density x 10^{+3} (amperes/square centimeter)	.612	.0612	.0551	.163	.612	.0612
Run Number	303	305	315	273	253	255

TABLE 11

Summary of Limiting Current Densities and Energy Efficiencies from Prototype Cell Experiments

Redox Couple	Fe-Ti	Fe-Ti	Fe-Ti	Fe-Ti	Fe-Ti	Fe-Ti
Concentration (moles/liter)	1	1	1	1	.25	.125
Temperature (°K)	310	330	310	310	310	310
Membrane	IM-12	3475	3475	AMV	AMV	AMV
Limiting Current Density x 10^{+3} (amperes/centimeter squared)	3.96	1.34	1.16	.376	3.00	1.25
Highest % Energy Efficiency	90+	40.8	55.8	90+	90+	90+
Load Resistance for Highest % Energy Efficiency (ohms)	1000	10	100	1000	100	1000
Lowest % Energy Efficiency	90+	5.15	29.3	90+	46.3	37.6
Load Resistance for Lowest % Energy Efficiency (ohms)	10	100	10	100	10	10

TABLE 11
(Continued)

Redox Couple	Fe-Sn	Fe-Sn	Fe-Sn	Sn-Cr	Sn-Cr	Sn-Cr
Concentration (moles/liter)	1	.5	.25	1	.5	.25
Temperature (°K)	310	310	310	310	310	310
Membrane	AMV	AMV	AMV	AMV	AMV	AMV
Limiting Current Density x 10^{+3} (amperes/centimeter squared)	.348	.0208	1.86	2.37	.315	3.96
Highest % Energy Efficiency	90+	90+	90+	90+	90+	90+
Load Resistance for Highest % Energy Efficiency (ohms)	1000	1000	1000	100	100	100
Lowest % Energy Efficiency	90+	6.1	54.4	76.9	90+	69.6
Load Resistance for Lowest % Energy Efficiency (ohms)	10	10	10	10	10	10

TABLE 11
(Concluded)

Redox Couple	Sn-Cr	Fe-Cr	Fe-Cr	Fe-Cr	Fe-Cr	Fe-Cr	Fe-Cr
Concentration (moles/liter)	.125	.5	1	1	.5	.25	1
Temperature (°K)	310	310	350	310	310	310	310
Membrane	AMV	AMV	3475	IM-12	065	065	183
Limiting Current Density x 10^{+3} (amperes/centimeter squared)	1.46	.858	.961	1.12	2.50	.673	.424
Highest % Energy Efficiency	90+	90+	64.2	90+	90+	90+	90+
Load Resistance for Highest % Energy Efficiency (ohms)	1000	1000	100	1000	100	1000	1000
Lowest % Energy Efficiency	29.8	18.8	10.7	14.9	39.4	90+	90+
Load Resistance for Lowest % Energy Efficiency (ohms)	10	10	1000	1000	10	100	100

SUMMARY

We consider our progress extremely well on this research under the sponsorship of NASA. The information obtained should be invaluable in the future development of this unique redox secondary battery system.

REFERENCES

1. Linke, W. F., Solubilities - Inorganic and Metal-Organic Compounds, ACS, Washington, D. C., 1958.

2. Lamb, A. B., J. of Am. Chem. Soc., 18, 1710, 1907.

3. Weast, R. C., ed., Handbook of Chemistry and Physics 48th Ed., pp. 13-169, Chemical Rubber Co., 1967.

4. Udy, M. J., Chromium - Volume 1 Chemistry of Chromium and Its Compounds,pp. 188-290, ACS Monograph Series, Reinhold Publishing Corp., New York, 1956.

5. Stone, H. W. and Beeson, C., Ind. Eng. Chem., Anal. Ed., 8, 188, 1936.

6. Lingane, J. J. and Pecsok, R. L., Anal. Chem., 20, 425, 1948.

7. Williams, R. L. and Sill, C. W., Anal. Chem., 46, 791, 1974.